International Journal of Non-Linear Mechanics 147 (2022) 104239

Contents lists available at ScienceDirect

International Journal of Non-Linear Mechanics

journal homepage: www.elsevier.com/locate/nlm

Hopf bifurcation calculation in neutral delay differential equations: Nonlinear robotic arms subject to delayed acceleration feedback control

Andras Bartfai *, Zoltan Dombovari

MTA-BME Lendület Machine Tool Vibration Research Group, Budapest University of Technology and Economics, Department of Applied Mechanics, Budapest, Hungary

ARTICLE INFO

Keywords:
Neutral delay differential equation
Hopf bifurcation
Delayed acceleration feedback control
Nonlinear robotic arm
Nonlinear control

ABSTRACT

This study gives the derivation of the Hopf bifurcation calculation for neutral delay differential equations using the centre manifold reduction theorem and normal form calculation. The whole concept was inspired by a case study where a robotic arm subjected to nonlinear stiffness with delayed acceleration feedback controller is modelled. Two different configurations are distinguished depending on the location of the acceleration sensor, a collocated and a non-collocated one. After a brief investigation of the linear stability, the bifurcation occurring at the loss of stability is calculated with the presented analytic equations for neutral delay differential equations. Then, a nonlinear term is introduced in the control law that can modify the occurring subcritical behaviour and improve the robustness of the system. The analytic results are carefully analysed and validated via a numerical continuation software, which also provided useful information about the global behaviour of the bifurcations in addition to the locally valid analytic results.

1. Introduction

There is a trend in the manufacturing industry to develop machining applications for robotic arms [1,2], which faces two main problems dynamically. Firstly, a robotic arm has a dynamically weak structure compared to dedicated machine tools and as such, it is prone to more significant nonlinear behaviour considering e.g. the same amplitude of oscillation. Secondly, machining processes like turning and milling are regenerative processes [3,4] as the past states of the dynamic system play an important role in the long-term behaviour of the mechanical system. Application of robotic arms in the industry is almost impossible without bypassing the dedicated control of the robot manufacturer, which is usually developed to have geometrical repeatability and accurate path following. These requirements are not especially adequate to control the robot during machining processes. This means that the only possibility is to apply machining operation control through the dedicated robot control, which results in a sluggish system with relatively large computation, sampling, and reaction delay.

The current study presents a seed development to mimic an acceleration feedback mechanism with the simplest possible model of a robotic arm through its dedicated position control by having the above-mentioned corresponding structural nonlinearity. Here, machining processes are not included due to their complexity, which must be dealt with numerically anyways, while its pure delayed nature is mathematically less challenging and already studied [5,6] than the introduced multi-degree-of-freedom neutral type system of the governing problem. On the road to accomplish machining of metal parts with robots, the first crucial step is to study the robot in itself with the nonlinear stiffness behaviour and additional acceleration feedback controller. This has to be achieved regardless of machining. We note that in later studies, the full problem has to be tackled including also machining, but the main motivation here is to carry out the analytical development of a multi-degree-of-freedom neutral system, which undergoes dynamic stability loss, corresponding to a Hopf bifurcation in the nonlinear system.

The analytical study of Hopf bifurcations is important in several aspects and can provide useful non-local information about the given dynamical system. Hopf bifurcation calculation can detect the presence of limit cycles caused by nonlinearity and predict their local nature existing 'around' the equilibrium or in other words the working point. The chance to get analytical or semi-analytical solutions to nonlinear problems is always promising, in comparison to numerical schemes that in their simple form serve as no more than numerical experiments. The obtained expressions of these calculations can reveal important parameter dependencies, which can be crucial for understanding how the applied control can counter-effect the present nonlinearity. Another issue with numerical solutions is that simulations cannot run backwards in time in the case of delayed or neutral systems. This prevents finding an unstable limit cycle in the same way as stable ones by simulating backwards.

* Corresponding author.
E-mail addresses: andras.bartfai@mm.bme.hu (A. Bartfai), dombovari@mm.bme.hu (Z. Dombovari).

https://doi.org/10.1016/j.ijnonlinmec.2022.104239
Received 8 February 2022; Received in revised form 8 August 2022; Accepted 11 September 2022
Available online 20 September 2022

As said before, the nonlinear behaviour of dynamical systems can be investigated with appropriate numerical methods. There are a large number of packages for the bifurcation analysis of systems of ordinary differential equations (ODEs). XPPAUTO [7] is a simulation and analysis package that provides an interface to AUTO [8], while DsTool [9] is an open source package that provides an interactive interface for all computations involving dynamical systems. PyDSTool [10] is designed for the replacement of DsTool, which provides tools for the simulation and analysis of dynamical systems, with a focus on biological applications. LOCBIF [11] is an interactive bifurcation analysis tool. The MATCONT [12] MATLAB package emerged out of CONTENT [13] that is an improved version of LOCBIF. The MATLAB-based continuation program COCO [14] is a development platform for continuation toolboxes.

Special methods are required to investigate retarded systems [15]. For retarded delay differential equations (RDDEs), the DDE-BIFTOOL [16] is a robust numerical continuation software based on MATLAB. Knut [17,18] is a graphical package for the analysis of RDDEs. For neutral delay differential equations (NDDEs) the NDDE-cont [19] numerical scheme was established as an extension to the DDE-BIFTOOL. The results of the numerical solutions must be validated with analytical solutions, whenever it is possible. Sometimes it is not an easy task to use these numerical schemes and evaluate the results depending on the investigated system. On the one hand, it can be problematic to initialize branches in numerical schemes. On the other hand with the help of analytical closed-form expressions, it is easy to obtain results for different parameter sets quickly. However, the analytical solutions are usually given by an expanded form, which is only a local approximation. This approximation is only valid locally, in the vicinity of the critical bifurcation point, and cannot give a good picture of the global behaviour. In comparison, numerical solutions give an efficient way to present the global picture of the bifurcations, but limited understanding of parameter dependency.

The Hopf (PAH) theorem for two-dimensional dynamical systems was derived by Andronov [20,21] which was suggested earlier by Poincaré [22]. The theorem was later proven by Hopf for arbitrary finite-dimensional systems [23]. Since then, it has been used in several applications [24,25]. The generalization of the Hopf bifurcation theorem to delay differential equations (DDEs) was done in [26]. Furthermore, an overview of the theorem can be found with results to simple examples in [27]. The first closed-form result was derived for a simple scalar RDDE [25], then results were published for vector RDDEs in [15,28]. Since then, several studies have been carried out for such systems, for example, [29] investigated nonlinearities in machine tool vibrations, [30] calculated double Hopf bifurcations in machining processes- and [31] investigated the nonlinear phenomena behind traffic with a car following model and time delays, just to mention a few. Furthermore, [32] gave a formal framework for the Hopf bifurcation calculation together with the centre manifold reduction for RDDEs.

Several studies can be found in the literature that investigates bifurcations in NDDEs. Among others, simple scalar neutral equations were studied in [33,34], neural-type neutral networks in [35], population models in [36], and circuit systems in [37]. Furthermore, symbolic calculations were presented in [38] together with the application to a controlled crane. However, a formal framework for the centre manifold reduction and normal form calculation of neutral delay differential equations is yet to be given. This study aims to fill in this gap.

The theory of Hopf bifurcation calculation in NDDEs was motivated by the nonlinear properties of a simple robotic arm with acceleration feedback control. A similar study was published on the topic [39], where the nonlinear behaviour of robots was investigated considering the time delay of the acceleration feedback controller as well. In that study, the analytical nonlinear properties were calculated with the method of multiple scales [40,41].

Industrial robots were first used in machining applications for clay prototyping [42,43] and later on for rapid prototyping [44,45] of plastic parts. Open kinematical chain robots have a versatile configuration with a large workspace, which makes them suitable for machining sculpture-like surfaces [46–48]. The disadvantage of this versatile configuration is that it usually lacks rigidity. At first, the design concept of robots focused on simple operations e.g. pick and place [49]. These tasks do not require extreme geometric accuracy, repeatability is a more important aspect here. The provided accuracy of stock robots was enough for the previously mentioned clay or plastic prototyping.

In contrast to the structural design of robots, machine tools usually do operations on metal parts. Their superstructure provides the necessary stiffness and rigidity [50], which is required for the sufficient geometrical accuracy of these operations. This results in robust and expensive structures, in contrast to robotic arms. Besides the required high accuracy in metal part machining, the reflected stiffness must overcome the so-called cutting stiffness [51], which is the minimum requirement for the stability of the operation. This is hard to achieve with industrial robots having slender and not particularly stiff robotic arms [52–54]. For this problem, stiffer designs of open kinematic chain robotic arms can be found, but these configurations can drastically reduce the workspace nullifying one of the main advantages of robotic manufacturing.

To upgrade the dynamic performance of the robot, an online control solution can be deployed using built-in velocity or acceleration feedback controllers. This can be problematic since the manufacturer usually does not provide access to the built-in controllers. Contrarily, the stock robots could be upgraded with the acceptance of the owners using off-line techniques or certified built-in control. A possible solution to increase the dynamic reflected stiffness of the end effector is to use mounted passive or semi-active embedded solutions. However, industrial robot users are usually not comfortable accepting these solutions. Another possible relatively simple and cheap solution can be utilized using additional feedback signals in the already built-in position control of the robot. To achieve stable manufacturing using the new feedback controller, careful parameter management and the synchronization of time delays with the built-in controller are necessary.

Acceleration feedback is a popular choice in industrial applications thanks to its simplicity. Consequently, in this study, an additional acceleration feedback controller is proposed, which is fed through the conventional built-in controller of the robot, which is usually a proportional–derivative controller [55], to mitigate the vibrations generated by the machining process [56–60] or to compensate for the flexibility of the robotic arm [61,62]. The use of feedback controllers commonly introduces time delays [15], which can have a non-negligible effect on the stability of the system. Even small time delays can considerably change the stability properties and the behaviour of dynamical systems [63,64].

A two degrees-of-freedom (DoF) lumped model of a nonlinear robotic arm subject to delayed acceleration feedback control is investigated here, inspired by [39]. In many studies the links of the robotic arm are modelled [65,66]. In other approaches the arms are modelled as continuum [67]. Our model is much simpler, so that we can focus on the instabilities generated by the additional acceleration feedback controller and derive closed form solutions. We consider this as the simplest possible equivalent model that can reproduce the nonlinear behaviour of the robotic arm together with the time delay of the acceleration feedback controller. A collocated and a non-collocated configuration are distinguished, based on the position of the acceleration sensor. The system is collocated if the sensor is near the actuator and non-collocated if it is near the end effector [68,69]. The stability of both configurations is briefly studied. Modelling the stiffness nonlinearity of the robot, a third-order polynomial function is introduced. Firstly, the main nonlinearity, which is the third-order term, is considered and the bifurcations occurring at the loss of stability are analytically studied with the Hopf bifurcation calculation derived for NDDEs. Then, a third-order nonlinear term is introduced in the control law to control the bifurcation in case of subcritical behaviour to improve the robustness. Finally, a second-order term is also introduced in the stiffness characteristic, which models the non-symmetric

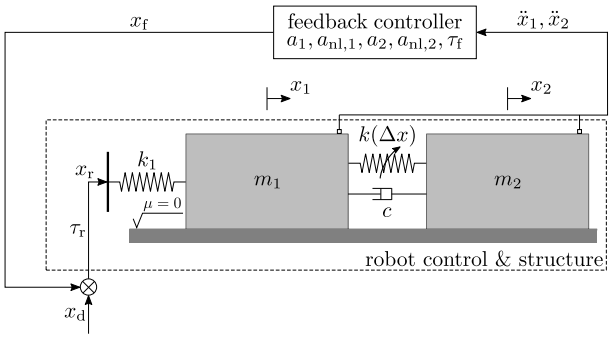

Fig. 1. Two degrees of freedom model of the robotic arm.

behaviour of the system. The effect of this non-symmetric term on the bifurcations is investigated with and without a nonlinear term in the control law. The analytical results are validated with the numerical solutions from the NDDE-cont continuation software. The advantages and limitations of the analytical and numerical solutions are carefully analysed and compared.

2. Mechanical model

A schematic of the adopted two DoF mechanical system can be seen in Fig. 1. The model consists of two lumped masses m_1 and m_2 connected by a nonlinear spring k and a linear damping c. The prescribed reference trajectory x_d is programmed, such that in ideal circumstances an identical constrained motion x_r is imposed to mass m_1 via a linear spring k_1 with time delay τ_r. This gives the dynamical system governed by the following equations of motion

$$\begin{aligned} &m_1\ddot{x}_1 + c(\dot{x}_1 - \dot{x}_2) + k(\Delta x)(x_1 - x_2) + k_1 x_1 = k_1 x_r, \\ &m_2\ddot{x}_2 + c(\dot{x}_2 - \dot{x}_1) + k(\Delta x)(x_2 - x_1) = 0, \end{aligned} \tag{1}$$

where x_1 and x_2 are the displacements of the lumped masses. Overdot $(\dot{})$ indicates derivation with respect to time t. Furthermore, $\Delta x := x_2 - x_1$ and the nonlinear spring is considered with a second-order nonlinearity in the stiffness characteristic $k(\Delta x) = k_2 + k_{nl,1}\Delta x + k_{nl,2}\Delta x^2$, which will lead to a third-order polynomial nonlinearity in the system. The physical interpretation of parameters $k_{nl,1}$ and $k_{nl,2}$ can be explained by the gear backlash phenomenon [70,71], which is related to the tolerances of the gear teeth resulting usually in stiffening behaviour. This plays an important role in robotic arms also, since the drives are usually gear-driven. The nonlinear behaviour of the backlash is often modelled with a third-order stiffness characteristic function [71]. In this sense, the parameter $k_{nl,2}$ corresponds to the main nonlinear characteristic of the drives of the robotic arms and $k_{nl,1}$ corresponds to a slight non-symmetric behaviour of the gear backlash. Apart from the prescribed reference trajectory x_d, an additional feedback signal x_f, including a third-order nonlinear acceleration term is fed back with time delay τ_f. In summary, this gives the ideal constrained motion x_r. The final constrained motion is $x_r(t) = x_d(t-\tau_r) + a_1\ddot{x}_1(t-\tau) + a_{nl,1}\ddot{x}_1^3(t-\tau) + a_2\ddot{x}_2(t-\tau) + a_{nl,2}\ddot{x}_2^3(t-\tau)$, where $\tau = \tau_r + \tau_f$ is the delay of the control force. The linear part of the control law is present to improve the dynamic performance of robots in future applications in machining. With the nonlinear part of the control law we aim to modify possible subcritical bifurcations to supercritical increasing the robustness of the system. The linear and nonlinear acceleration control gains are a_1, a_2, $a_{nl,1}$ and $a_{nl,2}$ respectively. The values m_1, m_2, c, k_1 and k_2 are assumed to be positive real numbers, while $k_{nl,1}$, $k_{nl,2}$, a_1, a_2, $a_{nl,1}$ and $a_{nl,2}$ are generic real numbers. We assume that the control force is calculated based on the value of the acceleration of mass m_1 or m_2; therefore, we assume that either $a_1 = 0$ and $a_{nl,1} = 0$ or $a_2 = 0$ and $a_{nl,2} = 0$. These two cases correspond to a non-collocated or collocated controller, respectively. With these considerations, the equations of motion can be written as

$$\begin{aligned} &m_1\ddot{x}_1 + c(\dot{x}_1 - \dot{x}_2) + k_2(x_1 - x_2) + k_1 x_1 - k_{nl,1}(x_1 - x_2)^2 \\ &\quad + k_{nl,2}(x_1 - x_2)^3 = k_1(x_{d\tau_r} + a_1\ddot{x}_{1\tau} + a_{nl,1}\ddot{x}_{1\tau}^3 + a_2\ddot{x}_{2\tau} + a_{nl,2}\ddot{x}_{2\tau}^3), \\ &m_2\ddot{x}_2 + c(\dot{x}_2 - \dot{x}_1) + k_2(x_2 - x_1) + k_{nl,1}(x_2 - x_1)^2 + k_{nl,2}(x_2 - x_1)^3 = 0, \end{aligned} \tag{2}$$

where $x_{d\tau r} = x_d(t-\tau_r)$, $\ddot{x}_{1\tau} = \ddot{x}_1(t-\tau)$, $\ddot{x}_{2\tau} = \ddot{x}_2(t-\tau)$. In order to focus on the instabilities induced by the acceleration feedback controller, constant prescribed reference trajectory is assumed $x_d(t) \equiv x_d$. This results in an equilibrium $(\overline{x}_1,\ \overline{x}_2) = (x_d,\ x_d)$. With the introduction of perturbations $x_1 = \overline{x}_1 + u_1$ and $x_2 = \overline{x}_2 + u_2$, the variation equations can be written as

$$\begin{aligned} &m_1\ddot{u}_1 + c(\dot{u}_1 - \dot{u}_2) + k_2(u_1 - u_2) + k_1 u_1 - k_{nl,1}(u_1 - u_2)^2 + k_{nl,2}(u_1 - u_2)^3 \\ &= k_1(a_1\ddot{u}_{1\tau} + a_{nl,1}\ddot{u}_{1\tau}^3 + a_2\ddot{u}_{2\tau} + a_{nl,2}\ddot{u}_{2\tau}^3), \\ &m_2\ddot{u}_2 + c(\dot{u}_2 - \dot{u}_1) + k_2(u_2 - \tilde{u}_1) + k_{nl,1}(u_2 - u_1)^2 + k_{nl,2}(u_2 - u_1)^3 = 0. \end{aligned} \tag{3}$$

In order to reduce the number of parameters, we divide both equations by m_1, obtaining the system

$$\begin{aligned} &\ddot{u}_1 + 2\chi r\omega_2(\dot{u}_1 - \dot{u}_2) + \omega_2^2 r(u_1 - u_2) + \omega_1^2 u_1 - \frac{k_{nl,1}}{m_1}(u_1 - u_2)^2 \\ &\quad + \frac{k_{nl,2}}{m_1}(u_1 - u_2)^3 - \omega_1^2(a_1\ddot{u}_{1\tau} + a_{nl,1}\ddot{u}_{1\tau}^3 + a_2\ddot{u}_{2\tau} + a_{nl,2}\ddot{u}_{2\tau}^3) = 0, \\ &\ddot{u}_2 + 2\chi\omega_2(\dot{u}_2 - \dot{u}_1) + \omega_2^2(u_2 - u_1) + \frac{k_{nl,1}}{r\,m_1}(u_2 - u_1)^2 + \frac{k_{nl,2}}{r\,m_1}(u_2 - u_1)^3 = 0, \end{aligned} \tag{4}$$

where $r := m_2/m_1$ is the mass ratio, $\omega_1 := \sqrt{k_1/m_1}$, $\omega_2 := \sqrt{k_2/m_2}$ are the angular natural frequencies of the standalone 1 DoF fixed spring systems and $\chi := c/(2m_2\omega_2)$ is the standalone damping ratio. Then, we introduce the dimensionless time $t\omega_1 \to t$ and displacements $u_1\sqrt{|k_{nl,2}|/(rk_1)} \to u_1$ and $u_2\sqrt{|k_{nl,2}|/(rk_1)} \to u_2$, reducing the system to

$$\begin{aligned} &u_1'' + 2\chi r\gamma(u_1' - u_2') + \gamma^2 r(u_1 - u_2) + u_1 - \nu\, r(u_1 - u_2)^2 + \sigma\, r(u_1 - u_2)^3 \\ &\quad - (\kappa_1 u_{1\tau}'' + \kappa_{nl,1}u_{1\tau}''^3 + \kappa_2 u_{2\tau}'' + \kappa_{nl,2}u_{2\tau}''^3) = 0, \\ &u_2'' + 2\chi\gamma(u_2' - u_1') + \gamma^2(u_2 - u_1) + \nu(u_2 - u_1)^2 + \sigma(u_2 - u_1)^3 = 0, \end{aligned} \tag{5}$$

where prime $(')$ indicates derivation with respect to the new, rescaled dimensionless time t, while $u_{1\tau}'' = u_1''(t-\tau)$, $u_{2\tau}'' = u_2''(t-\tau)$, with the dimensionless time delay $\tau\omega_1 \to \tau$. Besides, the dimensionless standalone natural frequency ratio $\gamma := \omega_2/\omega_1$, the rescaled control parameters $\kappa_1 := \omega_1^2 a_1$, $\kappa_2 := \omega_1^2 a_2$, the rescaled nonlinear control parameters $\kappa_{nl,1} := \omega_1^6 a_{nl,1} r\,k_1/|k_{nl,2}|$, $\kappa_{nl,2} := \omega_1^6 a_{nl,2} r\,k_1/|k_{nl,2}|$ and $\nu := (k_{nl,1}/\sqrt{r\,k_1})\sqrt{|1/k_{nl,2}|}$, $\sigma := \mathrm{sign}(k_{nl2})$.

3. Linear stability

The linear stability of the system can be investigated with the D-separation method [72]. The details of the calculation are omitted in this study. We refer to [39], where a similar system was investigated, which gives the same results for the linear stability as our system. With the D-separation method, the D-curves can be given, which define the critical (non-hyperbolic) boundaries. Stability boundaries are such critical boundaries, which surround the regions where the number of unstable characteristic exponents is zero. For the collocated case we impose $\kappa_2 = 0$ and solve the equations for the collocated control parameter κ_1, which gives (6) in Box I. In the non-collocated case $\kappa_1 = 0$ and we can solve for the non-collocated control parameter κ_2, which gives (7) in Box I.

Solving the equations obtained from the D-separation method with

$$\kappa_1 = \pm\sqrt{\frac{2\gamma^2\omega^2\left((r+1)\omega^2-1\right)\left(2\chi^2((r+1)\omega^2-1)-\omega^2+1\right)+\gamma^4((r+1)\omega^2-1)^2+\omega^4(\omega^2-1)^2}{\omega^4\left(2\left(2\chi^2-1\right)\gamma^2\omega^2+\gamma^4+\omega^4\right)}}, \tag{6}$$

$$\kappa_2 = \pm\sqrt{\frac{2\gamma^2\omega^2\left((r+1)\omega^2-1\right)\left(2\chi^2((r+1)\omega^2-1)-\omega^2+1\right)+\gamma^4((r+1)\omega^2-1)^2+\omega^4(\omega^2-1)^2}{\gamma^2\omega^4\left(4\chi^2\omega^2+\gamma^2\right)}}. \tag{7}$$

Box I.

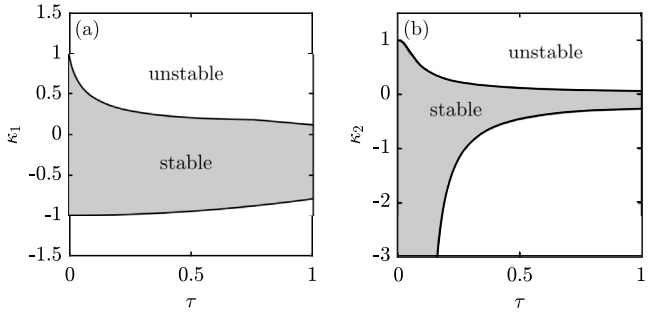

Fig. 2. Stability boundaries for the collocated (a) and non-collocated systems (b) with parameters $r = 1,\ \gamma = 1,\ \chi = 0.05$ in the plane of the control parameters $\kappa_1,\ \kappa_2$ and the time delay τ. The black line shows the stability boundary and the grey zone the stable region.

respect to $\sin\omega\tau$ and $\cos\omega\tau$, we obtain

$$\begin{aligned} s(\omega) &:= \sin\omega\tau = \frac{2\chi\gamma\omega\left(\kappa_1 r\omega^2-\kappa_2\omega^2+\kappa_2\right)}{d(\omega)}, \\ c(\omega) &:= \cos\omega\tau = \frac{1}{\omega^2\, d(\omega)}\left(\gamma^2\omega^2(\kappa_1(4\chi^2((r+1)\omega^2-1)-(r+2)\omega^2+2)\right. \\ &\quad + \kappa_2(4\chi^2((r+1)\omega^2-1)-\omega^2+1)) \\ &\quad \left. + \gamma^4(\kappa_1+\kappa_2)\left((r+1)\omega^2-1\right)+\kappa_1\omega^4(\omega^2-1)\right), \end{aligned} \tag{8}$$

where

$$d(\omega) := 2\gamma^2\omega^2(\kappa_1+\kappa_2)\left(\left(2\chi^2-1\right)\kappa_1+2\chi^2\kappa_2\right)+\gamma^4(\kappa_1+\kappa_2)^2+\kappa_1^2\omega^4. \tag{9}$$

From (8), we can directly obtain the value of τ as a function of ω, i.e.

$$\tau_n(\omega) = \frac{\operatorname{atan2}(s(\omega),\ c(\omega))+n\,2\pi}{\omega}, \qquad n\in\mathbb{Z}. \tag{10}$$

With these results, we can plot the stability boundaries. In the collocated case we use the $\kappa_1,\ \tau$ plane and in the non-collocated case, the $\kappa_2,\ \tau$ plane. The stability boundaries can be seen in Fig. 2. The detailed parameter analysis can be found in [39].

The nonlinear behaviour in robots is a non-negligible phenomenon. Subcritical Hopf bifurcation means that an unstable limit cycle emerges from the bifurcation point inside the stable region. From an engineering point of view, this behaviour usually has negative effects. This means that for a large enough perturbation the system can become unstable even though the system is stable for small perturbations. The flexible robotic arm can experience perturbations that can lead to such unstable vibrations. In the case of a supercritical Hopf bifurcation, a stable limit cycle emerges from the bifurcation point inside the unstable region. Contrary to subcritical behaviour, supercritical limit cycles are usually a favourable phenomenon, because they limit the vibration amplitude in an unstable parameter region. This means that they make the system more robust. In addition, they make the system safer in case of unexpected parameter changes. Consequently, the goal in the development of nonlinear controllers is to change the nature of the occurring Hopf bifurcations from subcritical to supercritical to increase the robustness of the system.

4. Hopf bifurcation calculation in neutral systems

In this section, we aim to give an overview of the normal form calculation of the Hopf bifurcation in neutral systems using the centre manifold reduction. Normal form theories aim to transform the system into a simpler form. Poincaré's theory of normal forms, which is also employed in this study, produces simple forms from differential equations in the neighbourhood of an equilibrium or periodic motion by means of power series expansion [73]. Additionally, the local long-term dynamics of the system is determined by the flow on a two-dimensional centre manifold embedded in the infinite-dimensional phase space of the delay differential equation [74]. Although there is a wide range of studies regarding the calculation of Hopf bifurcations in delayed systems, few studies carried out the calculation for neutral systems. Therefore, we present here a clear derivation of the centre manifold reduction and the Poincaré normal form for neutral delay differential equations. For the retarded case [32] gives a good overview of the Hopf bifurcation calculation.

4.1. Existence of the Hopf bifurcation

If two conditions are satisfied, then a Hopf bifurcation exists at the critical bifurcation value μ_{cr}. Firstly, at the critical bifurcation parameter value, μ_{cr} exists a complex conjugate pair of purely imaginary characteristic exponents

$$\lambda_{1,2}(\mu_{\mathrm{cr}}) = \pm\mathrm{i}\,\omega, \tag{11}$$

where $\omega \in \mathbb{R}^+$ is the frequency at the critical value of stability. The other condition is that the critical characteristic exponents $\lambda_{1,2}$ have to cross the imaginary axis with a nonzero speed by varying the bifurcation parameter μ

$$\mathrm{Re}\,\frac{\mathrm{d}\lambda(\mu)}{\mathrm{d}\mu}\bigg|_{\mu=\mu_{\mathrm{cr}}} \neq 0. \tag{12}$$

This derivative can be expressed via the implicit differentiation of the characteristic function with respect to the bifurcation parameter

$$\frac{\mathrm{d}D(\lambda(\mu);\ \mu)}{\mathrm{d}\mu} = \frac{\partial D(\lambda(\mu);\ \mu)}{\partial\mu} + \frac{\partial D(\lambda(\mu);\ \mu)}{\partial\lambda}\frac{\mathrm{d}\lambda(\mu)}{\mathrm{d}\mu}, \tag{13}$$

where $D(\lambda(\mu);\ \mu)$ is the characteristic function. Therefore, the critical characteristic exponent crosses the imaginary axis with speed

$$\mathrm{Re}\,\frac{\mathrm{d}\lambda(\mu)}{\mathrm{d}\mu}\bigg|_{\mu=\mu_{\mathrm{cr}}} = \mathrm{Re}-\left.\frac{\left.\frac{\partial D(\lambda(\mu);\ \mu)}{\partial\mu}\right|_{\mu=\mu_{\mathrm{cr}}}}{\left.\frac{\partial D(\lambda(\mu);\ \mu)}{\partial\lambda}\right|_{\mu=\mu_{\mathrm{cr}}}}\right|_{\lambda=\mathrm{i}\omega}. \tag{14}$$

For the collocated case, with κ_1 chosen as the bifurcation parameter the crossing speed is

$$\begin{aligned}\mathrm{Re}\left.\frac{\mathrm{d}\lambda(\mu)}{\mathrm{d}\mu}\right|_{\mu=\kappa_{1\mathrm{cr}}} &= (\omega^2(2\gamma\chi(\gamma^2((r+1)\omega^2-1)-3r\omega^4+\omega^4-\omega^2)\\ &\times\cos(\omega\tau)+\omega(\kappa_{1\mathrm{cr}}\omega(\gamma^3(\gamma\tau-2\chi)+2\gamma\omega^2(\gamma\tau(2\chi^2-1)-\chi)+\tau\omega^4)\\ &+2\sin(\omega\tau)(\gamma^4(r+1)+\gamma^2(\chi^2(6(r+1)\omega^2-2)-(r+3)\omega^2+1)\\ &+2\omega^4-\omega^2))))\Big/(4\gamma^2\chi^2+2\omega^6(\kappa_{1\mathrm{cr}}^2(\gamma\tau(\gamma\tau(2\chi^2-1)-2\chi)+8)+8)\\ &+\kappa_{1\mathrm{cr}}^2\tau^2\omega^8+4\omega^2(\gamma^4(\kappa_{1\mathrm{cr}}^2+(r+1)^2)-2\gamma^2(r+1)(3\chi^2-1)+1)\\ &+4\kappa_{1\mathrm{cr}}\omega(\omega\cos(\omega\tau)(\omega^2(\gamma(\tau\chi(\gamma^2(r+1)-1)-18\gamma(r+1)\chi^2+4\gamma\\ &\times(r+2))+4)-\gamma^2(\gamma\tau\chi+2\gamma^2(r+1)-6\chi^2+2)+\omega^4(\gamma(1-3r)\tau\chi\\ &-8))+\sin(\omega\tau)(-2\gamma^3\chi+\omega^4(\tau(\gamma^2(6(r+1)\chi^2-r-3)-1)-12\gamma r\chi)\\ &+\gamma\omega^2(\gamma\tau(\gamma^2(r+1)-2\chi^2+1)-2\chi)+2\tau\omega^6))+\omega^4(\gamma^4\kappa_{1\mathrm{cr}}^2\tau^2-4\gamma^3\\ &\times\kappa_{1\mathrm{cr}}^2\tau\chi+4\gamma^2(9\chi^2(\kappa_{1\mathrm{cr}}^2+(r+1)^2)-4(\kappa_{1\mathrm{cr}}^2+r+1))-16)).\end{aligned} \tag{15}$$

For the non-collocated case, with κ_2 chosen as the bifurcation parameter

$$\begin{aligned}\mathrm{Re}\left.\frac{\mathrm{d}\lambda(\mu)}{\mathrm{d}\mu}\right|_{\mu=\kappa_{2\mathrm{cr}}} &= (\gamma\omega^2(\gamma\omega(\kappa_{2\mathrm{cr}}\omega(\gamma^2\tau-2\gamma\chi+4\tau\chi^2\omega^2)+2\sin(\omega\tau)\\ &\times(\gamma^2(r+1)+\chi^2(6(r+1)\omega^2-2)-2\omega^2+1))+2\chi(\gamma^2((r+1)\omega^2-1)\\ &+4\omega^4-2\omega^2)\cos(\omega\tau)))\Big/(-4\gamma^3\kappa_{2\mathrm{cr}}^2\tau\chi\omega^4+\gamma^4\omega^2(\kappa_{2\mathrm{cr}}^2(\tau^2\omega^2+4)+4r\\ &\times(r+2)+4)+4\gamma^2(\chi^2(\kappa_{2\mathrm{cr}}^2\tau^2\omega^6+9\omega^4(\kappa_{2\mathrm{cr}}^2+(r+1)^2)-6(r+1)\omega^2\\ &+1)+2(r+1)\omega^2(1-2\omega^2))+4\gamma\kappa_{2\mathrm{cr}}\omega(\sin(\omega\tau)(-2\gamma^2\chi+\omega^2(\gamma\tau(\gamma^2(r\\ &+1)-2\chi^2+1)-6\chi)+2\omega^4(\gamma\tau(3(r+1)\chi^2-1)+6\chi))+\omega\cos(\omega\tau)\\ &\times(-\gamma(\gamma\tau\chi+2\gamma^2(r+1)-6\chi^2+2)+\omega^2(\gamma((r+1)\chi(\gamma\tau-18\chi)+4)\\ &-2\tau\chi)+4\tau\chi\omega^4))+4\omega^2(1-2\omega^2)^2).\end{aligned} \tag{16}$$

4.2. Centre manifold reduction

Neutral delay-differential equations in the form

$$\dot{\mathbf{u}}(t)=\mathbf{L}\,\mathbf{u}(t)+\mathbf{R}\,\dot{\mathbf{u}}(t-\tau)+\mathbf{F}(\mathbf{u}(t),\ \dot{\mathbf{u}}(t-\tau)), \tag{17}$$

where $\mathbf{L},\ \mathbf{R}\in\mathbb{R}^{n\times n}$ are constant matrices and $\mathbf{F}(\mathbf{u}(t),\ \dot{\mathbf{u}}(t-\tau))$ is an analytic function with the near-zero feature $\mathbf{F}(\mathbf{0},\ \mathbf{0})=\mathbf{0}$ can be rewritten at the critical bifurcation parameter as an operator differential equation on the Banach space $\mathscr{H}$ of continuously differentiable functions $\mathbf{u}:[-\tau,\ 0]\to\mathbb{R}^2$ as

$$\dot{\mathbf{u}}_t=\mathscr{A}\mathbf{u}_t+\mathscr{F}(\mathbf{u}_t), \tag{18}$$

where $\mathbf{u}_t\in\mathscr{H}$ is defined by the time shift

$$\mathbf{u}_t(\vartheta)=\mathbf{u}(t+\vartheta),\quad \vartheta\,[-\tau,\ 0]\,. \tag{19}$$

Generally, a $\mathbf{u}(t-\tau)$ term should also be included in (17) representing retarded terms. However, in our system this term is not present and the presented calculation can be easily extended to that case combining the results presented in this study and the well-known expressions of the retarded case. The linear operator $\mathscr{A}$ can be expressed as

$$\mathscr{A}\mathbf{u}(\vartheta)=\begin{cases}\mathbf{u}'(\vartheta), & \vartheta\in[-\tau,0),\\ \mathbf{L}\,\mathbf{u}(0)+\mathbf{R}\,\mathbf{u}'(-\tau), & \vartheta=0,\end{cases} \tag{20}$$

where $(')$ indicates derivation with respect to ϑ. The nonlinear operator $\mathscr{F}$ can be expressed as

$$\mathscr{F}(\mathbf{u})(\vartheta)=\begin{cases}\mathbf{0}, & \vartheta\in[-\tau,0),\\ \mathbf{F}(\mathbf{u}(0),\mathbf{u}'(-\tau)), & \vartheta=0.\end{cases} \tag{21}$$

The right-hand side critical eigenfunction $\mathbf{s}(\vartheta)$ of operator $\mathscr{A}$ corresponding to the critical characteristic roots $\lambda=\pm\mathrm{i}\omega$ satisfies

$$\begin{aligned}&\mathscr{A}\mathbf{s}(\vartheta)=\mathrm{i}\,\omega\,\mathbf{s}(\vartheta),\\ &\mathscr{A}\mathbf{s}^{\mathrm{H}}(\vartheta)=-\mathrm{i}\,\omega\,\mathbf{s}^{\mathrm{H}}(\vartheta),\end{aligned} \tag{22}$$

where the notation $\square^{\mathrm{H}}$ means the conjugate transpose. The real and imaginary part of the eigenfunction $\mathbf{s}(\vartheta)$ are $\mathbf{s}_{\mathrm{R}}(\vartheta)=\mathrm{Re}\,\mathbf{s}(\vartheta)$, $\mathbf{s}_{\mathrm{I}}(\vartheta)=\mathrm{Im}\,\mathbf{s}(\vartheta)$. Now the first row of (22) can be written as

$$\begin{aligned}&\mathscr{A}\mathbf{s}_{\mathrm{R}}(\vartheta)=-\omega\,\mathbf{s}_{\mathrm{I}}(\vartheta),\\ &\mathscr{A}\mathbf{s}_{\mathrm{I}}(\vartheta)=\omega\,\mathbf{s}_{\mathrm{R}}(\vartheta).\end{aligned} \tag{23}$$

From (23) we arrive to the linear ODE form for the critical eigenset

$$\begin{bmatrix}\mathbf{s}_{\mathrm{R}}'(\vartheta)\\ \mathbf{s}_{\mathrm{I}}'(\vartheta)\end{bmatrix}=\omega\begin{bmatrix}\mathbf{0} & -\mathbf{I}\\ \mathbf{I} & \mathbf{0}\end{bmatrix}\begin{bmatrix}\mathbf{s}_{\mathrm{R}}(\vartheta)\\ \mathbf{s}_{\mathrm{I}}(\vartheta)\end{bmatrix} \tag{24}$$

with defined boundary:

$$\begin{bmatrix}\mathbf{L} & \omega\mathbf{I}\\ -\omega\mathbf{I} & \mathbf{L}\end{bmatrix}\begin{bmatrix}\mathbf{s}_{\mathrm{R}}(0)\\ \mathbf{s}_{\mathrm{I}}(0)\end{bmatrix}+\begin{bmatrix}\mathbf{R} & \mathbf{0}\\ \mathbf{0} & \mathbf{R}\end{bmatrix}\begin{bmatrix}\mathbf{s}_{\mathrm{R}}'(-\tau)\\ \mathbf{s}_{\mathrm{I}}'(-\tau)\end{bmatrix}=\begin{bmatrix}\mathbf{0}\\ \mathbf{0}\end{bmatrix}, \tag{25}$$

where $\mathbf{I}\in\mathbb{R}^{n\times n}$ represents the identity matrix and $\mathbf{0}\in\mathbb{R}^{n\times n}$ is the zero matrix or the zero vector $\mathbf{0}\in\mathbb{R}^n$. The general solution of (24) can be written as

$$\begin{bmatrix}\mathbf{s}_{\mathrm{R}}(\vartheta)\\ \mathbf{s}_{\mathrm{I}}(\vartheta)\end{bmatrix}=\begin{bmatrix}\mathbf{S}_1\\ \mathbf{S}_2\end{bmatrix}\cos\omega\vartheta+\begin{bmatrix}-\mathbf{S}_2\\ \mathbf{S}_1\end{bmatrix}\sin\omega\vartheta, \tag{26}$$

where $\mathbf{S}_{1,2}\in\mathbb{R}^n$ are the coefficient vectors of the eigenfunctions $\mathbf{s}_{\mathrm{R,I}}$. It should be noted that $\mathbf{S}_{1,2}$ have two freely eligible variables as usual in eigenvector problems. Substituting the values at the boundary gives the following linear homogeneous algebraic equation

$$\begin{bmatrix}\mathbf{L}+\omega\mathbf{R}\sin\omega\tau & \omega\mathbf{I}-\omega\mathbf{R}\cos\omega\tau\\ -\omega\mathbf{I}+\omega\mathbf{R}\cos\omega\tau & \mathbf{L}+\omega\mathbf{R}\sin\omega\tau\end{bmatrix}\begin{bmatrix}\mathbf{S}_1\\ \mathbf{S}_2\end{bmatrix}=\begin{bmatrix}\mathbf{0}\\ \mathbf{0}\end{bmatrix}. \tag{27}$$

The eigenfunctions $\mathbf{s}_{\mathrm{R}}(\vartheta)$ and $\mathbf{s}_{\mathrm{I}}(\vartheta)$ span the centre (critical) subspace that is tangent to the two-dimensional centre manifold of the infinite-dimensional phase space. In order to project the system to the space spanned by $\mathbf{s}_{\mathrm{R}}(\vartheta)$ and $\mathbf{s}_{\mathrm{I}}(\vartheta)$ and to its complementary space we need the left-hand side critical eigenfunction of $\mathscr{A}$ denoted by $\mathbf{n}(\vartheta)$. For this, we need the adjoint operator $\mathscr{A}^*$ satisfying

$$\begin{aligned}&\mathscr{A}^*\mathbf{n}(\xi)=-\mathrm{i}\,\omega\,\mathbf{n}(\xi),\\ &\mathscr{A}^*\mathbf{n}^{\mathrm{H}}(\xi)=\mathrm{i}\,\omega\,\mathbf{n}^{\mathrm{H}}(\xi).\end{aligned} \tag{28}$$

With the help of a suitable definition for the bilinear form (inner product), the adjoint operator can be defined satisfying the formal adjoint problem

$$\langle\mathbf{u},\mathscr{A}\mathbf{v}\rangle=\langle\mathscr{A}^*\mathbf{u},\mathbf{v}\rangle. \tag{29}$$

The bilinear form for the neutral case is

$$\langle\mathbf{u}(\vartheta),\mathbf{v}(\vartheta)\rangle=\int_{-\tau}^{0}\mathbf{u}^{\mathrm{H}}(\vartheta+\tau)\,\mathbf{R}\,\mathbf{v}'(\vartheta)\,\mathrm{d}\vartheta+(\mathbf{u}^{\mathrm{H}}(0)-\mathbf{u}^{\mathrm{H}}(\tau)\,\mathbf{R})\,\mathbf{v}(0). \tag{30}$$

For the detailed derivation, see Appendix A. The bilinear form gives the definition of the adjoint operator

$$\mathscr{A}^*\mathbf{v}(\xi)=\begin{cases}-\mathbf{v}'(\xi), & \xi\in(0,\tau],\\ \mathbf{L}^{\mathrm{H}}\mathbf{v}(0)-\mathbf{R}^{\mathrm{H}}\mathbf{v}'(\tau), & \xi=0.\end{cases} \tag{31}$$

Now we can calculate the left-hand side critical eigenfunctions. The real and imaginary part of vector $\mathbf{n}(\vartheta)$ are $\mathbf{n}_{\mathrm{R}}(\vartheta)=\mathrm{Re}\,\mathbf{n}(\vartheta)$, $\mathbf{n}_{\mathrm{I}}(\vartheta)=\mathrm{Im}\,\mathbf{n}(\vartheta)$. The first row of (28) can be rewritten as

$$\begin{aligned}&\mathscr{A}^*\mathbf{n}_{\mathrm{R}}(\xi)=\omega\,\mathbf{n}_{\mathrm{I}}(\xi),\\ &\mathscr{A}^*\mathbf{n}_{\mathrm{I}}(\xi)=-\omega\,\mathbf{n}_{\mathrm{R}}(\xi).\end{aligned} \tag{32}$$

Rewriting it gives a similar ODE with defined boundary as in Eqs. (24), (25)

$$\begin{aligned}&\begin{bmatrix}\mathbf{n}_{\mathrm{R}}'(\xi)\\ \mathbf{n}_{\mathrm{I}}'(\xi)\end{bmatrix}=\omega\begin{bmatrix}\mathbf{0} & -\mathbf{I}\\ \mathbf{I} & \mathbf{0}\end{bmatrix}\begin{bmatrix}\mathbf{n}_{\mathrm{R}}(\xi)\\ \mathbf{n}_{\mathrm{I}}(\xi)\end{bmatrix},\\ &\begin{bmatrix}\mathbf{L}^{\mathrm{H}} & -\omega\mathbf{I}\\ \omega\mathbf{I} & \mathbf{L}^{\mathrm{H}}\end{bmatrix}\begin{bmatrix}\mathbf{n}_{\mathrm{R}}(0)\\ \mathbf{n}_{\mathrm{I}}(0)\end{bmatrix}-\begin{bmatrix}\mathbf{R}^{\mathrm{H}} & \mathbf{0}\\ \mathbf{0} & \mathbf{R}^{\mathrm{H}}\end{bmatrix}\begin{bmatrix}\mathbf{n}_{\mathrm{R}}'(-\tau)\\ \mathbf{n}_{\mathrm{I}}'(-\tau)\end{bmatrix}=\begin{bmatrix}\mathbf{0}\\ \mathbf{0}\end{bmatrix}.\end{aligned} \tag{33}$$

The general solution of (33) can be written as

$$\begin{bmatrix}\mathbf{n}_{\mathrm{R}}(\xi)\\ \mathbf{n}_{\mathrm{I}}(\xi)\end{bmatrix}=\begin{bmatrix}\mathbf{N}_1\\ \mathbf{N}_2\end{bmatrix}\cos\omega\xi+\begin{bmatrix}-\mathbf{N}_2\\ \mathbf{N}_1\end{bmatrix}\sin\omega\xi, \tag{34}$$

where $\mathbf{N}_{1,2} \in \mathbb{R}^n$ are the coefficient vectors, having two freely eligible variables. Substituting the values at the boundary gives the following linear homogeneous algebraic equation

$$\begin{bmatrix} \mathbf{L}^{\mathrm{H}} + \omega\,\mathbf{R}^{\mathrm{H}} \sin\omega\tau & -\omega\,\mathbf{I} + \omega\,\mathbf{R}\cos\omega\tau \\ \omega\,\mathbf{I} - \omega\,\mathbf{R}^{\mathrm{H}}\cos\omega\tau & \mathbf{L}^{\mathrm{H}} + \omega\,\mathbf{R}^{\mathrm{H}}\sin\omega\tau \end{bmatrix} \begin{bmatrix} \mathbf{N}_1 \\ \mathbf{N}_2 \end{bmatrix} = \begin{bmatrix} \mathbf{0} \\ \mathbf{0} \end{bmatrix}. \tag{35}$$

Using the bilinear form in (A.4), two orthonormal conditions can be defined as

$$\langle \mathbf{n}_{\mathrm{R}},\, \mathbf{s}_{\mathrm{R}} \rangle = 1, \qquad \langle \mathbf{n}_{\mathrm{R}},\, \mathbf{s}_{\mathrm{I}} \rangle = 0. \tag{36}$$

This gives two more equations, which can be rearranged for $\mathbf{N}_{1,2}$ as

$$\frac{1}{2}\begin{bmatrix} \mathbf{S}_1^{\mathrm{H}}(2\,\mathbf{I} + \mathbf{R}^{\mathrm{H}}(\omega\tau\sin\omega\tau - 2\cos\omega\tau)) - \mathbf{S}_2^{\mathrm{H}}\mathbf{R}^{\mathrm{H}}(\omega\tau\cos\omega\tau + \sin\omega\tau) \\ \mathbf{S}_1^{\mathrm{H}}\mathbf{R}^{\mathrm{H}}(\omega\tau\cos\omega\tau + \sin\omega\tau) + \mathbf{S}_2^{\mathrm{H}}(2\,\mathbf{I} + \mathbf{R}^{\mathrm{H}}(\omega\tau\sin\omega\tau - 2\cos\omega\tau)) \\ \mathbf{S}_1^{\mathrm{H}}\mathbf{R}^{\mathrm{H}}(\omega\tau\cos\omega\tau + \sin\omega\tau) + \mathbf{S}_2^{\mathrm{H}}\mathbf{R}^{\mathrm{H}}\omega\tau\sin\omega\tau \\ -\mathbf{S}_1^{\mathrm{H}}\mathbf{R}^{\mathrm{H}}\omega\tau\sin\omega\tau + \mathbf{S}_2^{\mathrm{H}}\mathbf{R}^{\mathrm{H}}(\omega\tau\cos\omega\tau + \sin\omega\tau) \end{bmatrix}^{\mathrm{T}} \begin{bmatrix} \mathbf{N}_1 \\ \mathbf{N}_2 \end{bmatrix} = \begin{bmatrix} 1 \\ 0 \end{bmatrix}. \tag{37}$$

Note that Eqs. (27), (35), (37) give $k = 2n + 2$ equations to solve. After the decomposition of the solution $\mathbf{u}_t(\vartheta)$ into the components $z_{1,2} : \mathbb{R} \to \mathbb{R}$ tangent to the centre subspace and into the infinite-dimensional component $\mathbf{w} : \mathbb{R} \to \mathbb{X}_{\mathbb{R}^n}$ transverse to the centre subspace and writing the equations into a truncated Taylor series form, we get

$$\begin{aligned} \begin{bmatrix} \dot z_1 \\ \dot z_2 \\ \dot{\mathbf{w}} \end{bmatrix} &= \begin{bmatrix} 0 & \omega & 0 \\ -\omega & 0 & 0 \\ 0 & 0 & \mathscr{A} \end{bmatrix} \begin{bmatrix} z_1 \\ z_2 \\ \mathbf{w} \end{bmatrix} + \begin{bmatrix} \sum_{j,k\geq 0}^{j+k=2,3} f_{jk0}^{(1)} z_1^j z_2^k \\ \sum_{j,k\geq 0}^{j+k=2,3} f_{jk0}^{(2)} z_1^j z_2^k \\ \sum_{j,k\geq 0}^{j+k=2} \left(\mathbf{f}_{jk0}^{(3c)} \cos\omega\vartheta + \mathbf{f}_{jk0}^{(3s)} \sin\omega\vartheta \right) z_1^j z_2^k \end{bmatrix} \\ &+ \begin{bmatrix} \sum_{i=1}^{n} \left(f_{101,i}^{(10)} z_1 + f_{011,i}^{(10)} z_2 \right) w_i(0) + \left(f_{101,i}^{(1\tau)} z_1 + f_{011,i}^{(1\tau)} z_2 \right) w_i'(-\tau) \\ \sum_{i=1}^{n} \left(f_{101,i}^{(20)} z_1 + f_{011,i}^{(20)} z_2 \right) w_i(0) + \left(f_{101,i}^{(2\tau)} z_1 + f_{011,i}^{(2\tau)} z_2 \right) w_i'(-\tau) \\ \begin{cases} \mathbf{0}, & \vartheta \in [-\tau, 0)\,, \\ \sum_{j,k\geq 0}^{j+k=2} \mathbf{f}_{jk0}^{(3)}, & \vartheta = 0 \end{cases} \end{bmatrix}, \end{aligned} \tag{38}$$

For the detailed derivation of this form and for the expressions of the coefficient terms see Appendix B.

4.3. Two-dimensional centre manifold

The centre manifold is tangent to the plane spanned by z_1 and z_2. Generally, second-order expansion of the centre manifold is needed. The second-order Taylor expansion of the centre manifold yields

$$\mathbf{w}(z_1, z_2)(\vartheta) = \frac{1}{2}(\mathbf{h}_{20}(\vartheta)\, z_1^2 + 2\mathbf{h}_{11}(\vartheta)\, z_1 z_2 + \mathbf{h}_{02}(\vartheta)\, z_2^2). \tag{39}$$

The unknown terms are $\mathbf{h}_{20}, \mathbf{h}_{11}, \mathbf{h}_{02} \in \mathbb{X}_{\mathbb{R}^n}$. Taking the derivative of (39) with respect to time yields

$$\dot{\mathbf{w}}(z_1, z_2)(\vartheta) = -\omega\,\mathbf{h}_{11}(\vartheta)\, z_1^2 + \omega\,(\mathbf{h}_{20}(\vartheta) - \mathbf{h}_{02}(\vartheta))\, z_1 z_2 + \omega\,\mathbf{h}_{11}(\vartheta)\, z_2^2. \tag{40}$$

On the other hand with

$$\mathscr{A}\mathbf{w} = \begin{cases} \frac{1}{2}(\mathbf{h}_{20}'(\vartheta)\, z_1^2 + 2\,\mathbf{h}_{11}'(\vartheta)\, z_1 z_2 + \mathbf{h}_{02}'(\vartheta)\, z_2^2), & \vartheta \in [-\tau, 0)\,, \\ \mathbf{L}\mathbf{w}(0) + \mathbf{R}\mathbf{w}'(-\tau), & \vartheta = 0. \end{cases} \tag{41}$$

Eq. (B.3) gives

$$\begin{aligned} \dot{\mathbf{w}}(z_1, z_2)(\vartheta) = &\frac{1}{2}(\mathbf{h}_{20}'(\vartheta)\, z_1^2 + 2\,\mathbf{h}_{11}'(\vartheta)\, z_1 z_2 + \mathbf{h}_{02}'(\vartheta)\, z_2^2) \\ &+ \sum_{j,k\geq 0}^{j+k=2} \left(\mathbf{f}_{jk0}^{(3c)} \cos\omega\vartheta + \mathbf{f}_{jk0}^{(3s)} \sin\omega\vartheta \right) z_1^j z_2^k. \end{aligned} \tag{42}$$

Comparing the coefficients of Eqs. (40) and (42) gives the system of differential equations

$$\begin{bmatrix} \mathbf{h}_{20}'(\vartheta) \\ \mathbf{h}_{11}'(\vartheta) \\ \mathbf{h}_{02}'(\vartheta) \end{bmatrix} = \begin{bmatrix} \mathbf{0} & -2\,\omega\,\mathbf{I} & \mathbf{0} \\ \omega\,\mathbf{I} & \mathbf{0} & -\omega\,\mathbf{I} \\ \mathbf{0} & 2\,\omega\,\mathbf{I} & \mathbf{0} \end{bmatrix} \begin{bmatrix} \mathbf{h}_{20}(\vartheta) \\ \mathbf{h}_{11}(\vartheta) \\ \mathbf{h}_{02}(\vartheta) \end{bmatrix} - \begin{bmatrix} 2\,\mathbf{f}_{200}^{(3c)} \\ \mathbf{f}_{110}^{(3c)} \\ 2\,\mathbf{f}_{020}^{(3c)} \end{bmatrix} \cos\omega\vartheta - \begin{bmatrix} 2\,\mathbf{f}_{200}^{(3s)} \\ \mathbf{f}_{110}^{(3s)} \\ 2\,\mathbf{f}_{020}^{(3s)} \end{bmatrix} \sin\omega\vartheta \tag{43}$$

with the boundary conditions

$$\begin{aligned} &\begin{bmatrix} \mathbf{L} & 2\,\omega\,\mathbf{I} & \mathbf{0} \\ -\omega\,\mathbf{I} & \mathbf{L} & \omega\,\mathbf{I} \\ \mathbf{0} & -2\,\omega\,\mathbf{I} & \mathbf{L} \end{bmatrix} \begin{bmatrix} \mathbf{h}_{20}(0) \\ \mathbf{h}_{11}(0) \\ \mathbf{h}_{02}(0) \end{bmatrix} + \begin{bmatrix} \mathbf{0} & -2\,\omega\,\mathbf{R} & \mathbf{0} \\ \omega\,\mathbf{R} & \mathbf{0} & -\omega\,\mathbf{R} \\ \mathbf{0} & 2\,\omega\,\mathbf{R} & \mathbf{0} \end{bmatrix} \begin{bmatrix} \mathbf{h}_{20}(-\tau) \\ \mathbf{h}_{11}(-\tau) \\ \mathbf{h}_{02}(-\tau) \end{bmatrix} \\ &= \begin{bmatrix} 2\,\mathbf{R}\,\mathbf{f}_{200}^{(3c)} \cos\omega\tau - 2\,\mathbf{R}\,\mathbf{f}_{200}^{(3s)} \sin\omega\tau - 2\,\mathbf{f}_{200}^{(3c)} - 2\,\mathbf{f}_{200}^{(3)} \\ \mathbf{R}\,\mathbf{f}_{110}^{(3c)} \cos\omega\tau - \mathbf{R}\,\mathbf{f}_{110}^{(3s)} \sin\omega\tau - \mathbf{f}_{110}^{(3c)} - \mathbf{f}_{110}^{(3)} \\ 2\,\mathbf{R}\,\mathbf{f}_{020}^{(3c)} \cos\omega\tau - 2\,\mathbf{R}\,\mathbf{f}_{020}^{(3s)} \sin\omega\tau - 2\,\mathbf{f}_{020}^{(3c)} - 2\,\mathbf{f}_{020}^{(3)} \end{bmatrix}. \end{aligned} \tag{44}$$

The general solution of (43) is

$$\begin{aligned} \begin{bmatrix} \mathbf{h}_{20}(\vartheta) \\ \mathbf{h}_{11}(\vartheta) \\ \mathbf{h}_{02}(\vartheta) \end{bmatrix} &= \begin{bmatrix} \mathbf{H}_0 \\ \mathbf{0} \\ \mathbf{H}_0 \end{bmatrix} + \begin{bmatrix} \mathbf{H}_1 \\ \mathbf{H}_2 \\ -\mathbf{H}_1 \end{bmatrix} \cos 2\omega\vartheta + \begin{bmatrix} -\mathbf{H}_2 \\ \mathbf{H}_1 \\ \mathbf{H}_2 \end{bmatrix} \sin 2\omega\vartheta \\ &+ \frac{2}{3\omega}\left(\begin{bmatrix} \mathbf{f}_{110}^{(3c)} + \mathbf{f}_{200}^{(3s)} + 2\,\mathbf{f}_{020}^{(3s)} \\ -\frac{1}{2}\mathbf{f}_{110}^{(3s)} - \mathbf{f}_{200}^{(3c)} + \mathbf{f}_{020}^{(3c)} \\ -\mathbf{f}_{110}^{(3c)} + 2\,\mathbf{f}_{200}^{(3s)} + \mathbf{f}_{020}^{(3s)} \end{bmatrix} \cos\omega\vartheta + \begin{bmatrix} \mathbf{f}_{110}^{(3s)} - \mathbf{f}_{200}^{(3c)} - 2\,\mathbf{f}_{020}^{(3c)} \\ \frac{1}{2}\mathbf{f}_{110}^{(3c)} - \mathbf{f}_{200}^{(3s)} + \mathbf{f}_{020}^{(3s)} \\ -\mathbf{f}_{110}^{(3s)} - 2\,\mathbf{f}_{200}^{(3c)} - \mathbf{f}_{020}^{(3c)} \end{bmatrix} \sin\omega\vartheta \right). \end{aligned} \tag{45}$$

Substituting back the boundary conditions and rearranging the equations give

$$\begin{aligned} &\begin{bmatrix} \mathbf{L} & \mathbf{0} & \mathbf{0} \\ \mathbf{0} & \mathbf{L} + 2\,\omega\,\mathbf{R}\sin 2\omega\tau & 2\omega\,\mathbf{I} - 2\,\omega\,\mathbf{R}\cos 2\omega\tau \\ \mathbf{0} & -2\,\omega\,\mathbf{I} + 2\,\omega\,\mathbf{R}\cos 2\omega\tau & \mathbf{L} + 2\,\omega\,\mathbf{R}\sin 2\omega\tau \end{bmatrix} \begin{bmatrix} \mathbf{H}_0 \\ \mathbf{H}_1 \\ \mathbf{H}_2 \end{bmatrix} \\ &= -\begin{bmatrix} \mathbf{f}_{200}^{(3)} + \mathbf{f}_{020}^{(3)} \\ \mathbf{f}_{200}^{(3)} - \mathbf{f}_{020}^{(3)} \\ \mathbf{f}_{110}^{(3)} \end{bmatrix} + \frac{2}{6\omega}\begin{bmatrix} (\mathbf{L} + \omega\,\mathbf{R}\sin\omega\tau)\left(-3\,\mathbf{f}_{200}^{(3s)} - 3\,\mathbf{f}_{020}^{(3s)} \right) \\ (\mathbf{L} + \omega\,\mathbf{R}\sin\omega\tau)\left(\mathbf{f}_{200}^{(3s)} - \mathbf{f}_{020}^{(3s)} - 2\mathbf{f}_{110}^{(3c)} \right) \\ (\mathbf{L} + \omega\,\mathbf{R}\sin\omega\tau)\left(2\,\mathbf{f}_{200}^{(3c)} - 2\,\mathbf{f}_{020}^{(3c)} + \mathbf{f}_{110}^{(3s)} \right) \\ \quad + (\omega\,\mathbf{I} - \omega\,\mathbf{R}\cos\omega\tau)\left(-3\,\mathbf{f}_{020}^{(3c)} - 3\,\mathbf{f}_{200}^{(3c)} \right) \\ \quad + (\omega\,\mathbf{I} - \omega\,\mathbf{R}\cos\omega\tau)\left(\mathbf{f}_{200}^{(3c)} - \mathbf{f}_{020}^{(3c)} + 2\,\mathbf{f}_{110}^{(3s)} \right) \\ \quad + (\omega\,\mathbf{I} - \omega\,\mathbf{R}\cos\omega\tau)\left(-2\,\mathbf{f}_{200}^{(3s)} + 2\,\mathbf{f}_{020}^{(3s)} + \mathbf{f}_{110}^{(3c)} \right) \end{bmatrix}. \end{aligned} \tag{46}$$

With this, the truncated form of $\mathbf{w}(\vartheta)$ can be calculated. Substituting back $\mathbf{w}(0)$ and $\mathbf{w}'(-\tau)$ gives, the two-dimensional centre manifold spanned by z_1 and z_2. Therefore, the derivative of $\mathbf{w}$ with respect to ϑ has to be calculated as well.

$$\mathbf{w}'(\vartheta) = \frac{1}{2}(\mathbf{h}_{20}'(\vartheta)\, z_1^2 + 2\,\mathbf{h}_{11}'(\vartheta)\, z_1 z_2 + \mathbf{h}_{02}'(\vartheta)\, z_2^2). \tag{47}$$

4.4. Poincaré normal form

The two-dimensional centre manifold can be written in the form

$$\begin{bmatrix} \dot z_1 \\ \dot z_2 \end{bmatrix} = \begin{bmatrix} 0 & \omega \\ -\omega & 0 \end{bmatrix} \begin{bmatrix} z_1 \\ z_2 \end{bmatrix} + \begin{bmatrix} \sum_{j,k\geq 0}^{j+k=2,3} a_{jk}^{(1)} z_1^j z_2^k \\ \sum_{j,k\geq 0}^{j+k=2,3} a_{jk}^{(2)} z_1^j z_2^k \end{bmatrix}, \tag{48}$$

where $a_{jk}^{(1)},\ a_{jk}^{(2)} \in \mathbb{R}$ are the corresponding constant coefficients in $z_1^j z_2^k$. With the coefficients of the Poincaré normal form, the Poincaré–Lyapunov coefficient can be calculated with the Bautin formula [15] as

$$\Delta = \frac{1}{8\omega}\left((a_{20}^{(1)} + a_{02}^{(1)})(-a_{11}^{(1)} + a_{20}^{(2)} - a_{02}^{(2)}) + (a_{20}^{(2)} + a_{02}^{(2)})(a_{20}^{(1)} - a_{02}^{(1)} + a_{11}^{(2)})\right) + \frac{1}{8}\left(3a_{30}^{(1)} + a_{12}^{(1)} + a_{21}^{(2)} + 3a_{03}^{(2)}\right). \tag{49}$$

The sign of the Poincaré–Lyapunov constant determines the type of the Hopf bifurcation. If $\Delta < 0$, then the bifurcation is supercritical, while in the case of $\Delta > 0$, the bifurcation is subcritical. The amplitude of the oscillation is expressed as

$$A = \sqrt{-\frac{1}{\Delta}\mathrm{Re}\frac{\mathrm{d}\lambda_{1,2}(\mu_{\mathrm{cr}})}{\mathrm{d}\mu}(\mu - \mu_{\mathrm{cr}})}. \tag{50}$$

The first Fourier term of the oscillation of the centre manifold can be calculated as

$$\begin{bmatrix} z_1(t) \\ z_2(t) \end{bmatrix} = A \begin{bmatrix} \cos\omega t \\ -\sin\omega t \end{bmatrix}. \tag{51}$$

By definition it is true that $\mathbf{u}(t) = \mathbf{u}_t(0)$ not too far from the critical bifurcation parameter. Therefore, the periodic solution in the vicinity of the bifurcation can be expressed as

$$\begin{aligned} &\mathbf{u}_t(\vartheta) \approx z_1(t)\,\mathbf{s}_{\mathrm{R}}(\vartheta) + z_2(t)\,\mathbf{s}_{\mathrm{I}}(\vartheta), \\ &\mathbf{u}(t) = \mathbf{u}_t(0) \approx z_1(t)\,\mathbf{s}_{\mathrm{R}}(0) + z_2(t)\,\mathbf{s}_{\mathrm{I}}(0) = A\,(\mathbf{S}_1\cos\omega t - \mathbf{S}_2\sin\omega t). \end{aligned} \tag{52}$$

5. Odd cubic stiffness nonlinearity

In this section, we neglect the second-order term of the nonlinear stiffness, which means that $\nu = 0$ in (5), so we can focus on the effect of the third-order term, whose coefficient is σ. The resulting nonlinearity will be an odd function. This means that the Hopf bifurcation can be directly calculated from the first two rows of (38) and it is not necessary to calculate the truncated form of $\mathbf{w}$. The centre manifold reduction and Poincaré normal form calculations are quite complicated. Therefore, the results of these calculations are not presented here. However, the Hopf bifurcation calculation can be done analytically and the expressions for the Poincaré–Lyapunov constant can be given in closed form. The results from the analytical calculations are verified with the NDDE-cont [19] continuation software for neutral delay differential equations. First, we analyse the collocated and non-collocated systems neglecting the nonlinear control parameter so that the effect of the nonlinear stiffness can be investigated. Then, with the introduction of the nonlinear control parameter, we try to influence the Hopf bifurcation in order to increase the robustness of the system.

5.1. Collocated case

Firstly, we analyse the collocated case, which means that the non-collocated control parameters are zero $\kappa_2 = 0$, $\kappa_{\mathrm{nl},2} = 0$.

5.1.1. Linear control

In this section, we set the nonlinear control parameter zero ($\kappa_{\mathrm{nl},1} = 0$) and investigate the effect of the cubic nonlinearity in the stiffness. In Figs. 3(i) the value of the Poincaré–Lyapunov constant Δ is plotted against the time delay τ for (a) hardening stiffness nonlinearity ($\sigma = 1$) and (b) softening stiffness nonlinearity ($\sigma = -1$). In Figs. 3(ii) the bifurcations can be seen for a given parameter set for (a) positive critical control parameter $\kappa_{1\mathrm{cr}} > 0$ (b) negative critical control parameter $\kappa_{1\mathrm{cr}} < 0$. In this case, the Poincaré Lyapunov constant has a simple linear dependence on the coefficient of the third-order stiffness σ:

$$\Delta = C_\sigma \sigma, \tag{53}$$

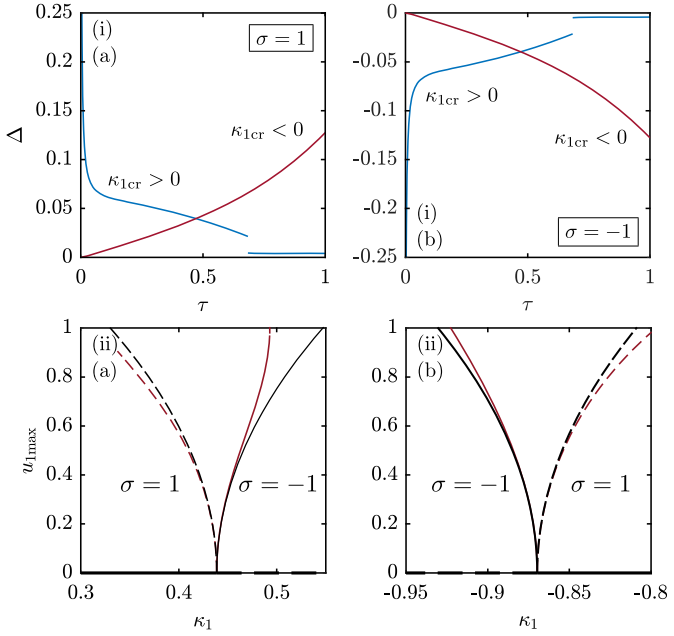

Fig. 3. (i) Poincaré–Lyapunov constant Δ of the collocated system against the time delay τ with linear collocated control for (a) hardening stiffness nonlinearity ($\sigma = 1$); (b) softening stiffness nonlinearity ($\sigma = -1$). The blue line represents the upper stability boundary, where the critical collocated control parameter is positive $\kappa_{1\mathrm{cr}} > 0$ and the red line the lower stability boundary, where it is negative $\kappa_{1\mathrm{cr}} < 0$. (ii) shows the bifurcations for (a) $\kappa_{1\mathrm{cr}} > 0$ and time delay $\tau = 0.1$; (b) $\kappa_{1\mathrm{cr}} < 0$ and time delay $\tau = 0.8$. The black line represents the analytical solution and the red one the numerical result. The bifurcations are subcritical ($\Delta > 0$) for hardening stiffness nonlinearity ($\sigma = 1$) and supercritical ($\Delta < 0$) for softening stiffness nonlinearity ($\sigma = -1$). Continuous and dashed curves show supercritical and subcritical branches respectively. The parameters are $r = 1$, $\gamma = 1$, $\chi = 0.05$. (For interpretation of the references to colour in this figure legend, the reader is referred to the web version of this article.)

where C_σ depends on the other parameters and in this case can be written as

$$\begin{aligned} C_\sigma = {} & (3r\omega^{10}(8\gamma^3\chi + \gamma^4\tau((r+1)\omega^2 - 1) + \gamma^2\tau\omega^2(-\omega^2(4(r+1)\chi^2 + r \\ & + 2) + 4\chi^2 + 2) + 2\gamma\chi\omega^2(r\omega^2 - 4) + \tau\omega^4(\omega^2 - 1)))\big/(4(\gamma^4 + 2\gamma^2 \\ & \times (2\chi^2 - 1)\omega^2 + \omega^4)(\gamma^4\omega^4(2\omega^4(2r^2 - 3(r+2)\tau^2) + 16\chi^4(\tau^2\omega^2((r \\ & + 1)\omega^2 - 1)^2 + 4) + 8\chi^2(\tau^2\omega^2(-(r+1)(r+2)\omega^4 + (3r+4)\omega^2 \\ & - 2) - 8) + (r(r+6)+6)\tau^2\omega^6 + 2\omega^2(3\tau^2 - 8r) + 24) + 2\gamma^2\omega^6(2\chi^2 \\ & \times (\omega^4(r^2 - 2(r+2)\tau^2) + (r(r+2)+2)\tau^2\omega^6 + 2\omega^2(\tau^2 - 4r) + 8) \\ & + \tau^2\omega^4(-(r+2)\omega^2 + r + 4) + 4r\omega^2 - 2\tau^2\omega^2 - 8) + \gamma^8(\tau^2\omega^2((r+1) \\ & \times\omega^2 - 1)^2 + 4) + 2\gamma^6\omega^2(4\chi^2(\tau^2\omega^2((r+1)\omega^2 - 1)^2 + 4) + \tau^2\omega^4(-(r \\ & + 1)(r+2)\omega^2 + 3r + 4) + 4r\omega^2 - 2\tau^2\omega^2 - 8) - 4\gamma^5 r\tau\chi\omega^6(3(r+1) \\ & \times \omega^2 - 5) + 4\gamma^3 r\tau\chi\omega^8(\omega^2(-4(r+1)\chi^2 + r + 2) + 12\chi^2 - 6) + 4\gamma r\tau \\ & \times \chi(\omega^2 + 1)\omega^{10} + \omega^8(\tau^2\omega^2(\omega^2 - 1)^2 + 4))). \end{aligned} \tag{54}$$

Fig. 3 shows that for hardening stiffness nonlinearity ($\sigma = 1$), the bifurcations are subcritical ($\Delta > 0$) in the investigated parameter region for both the upper ($\kappa_{1\mathrm{cr}} > 0$) and lower stability ($\kappa_{1\mathrm{cr}} < 0$) boundaries. For softening nonlinearity ($\sigma = -1$), the bifurcations are supercritical ($\Delta < 0$) for both stability boundaries showed in Fig. 2. As a result, hardening behaviour can limit the robustness of the system. In this case, a large enough perturbation can drive the system outside the unstable limit cycle. In Figs. 3(ii) the black and red lines are the analytical and numerical results respectively. The numerical solutions validate the analytical curves. In the vicinity of the critical bifurcation parameter, the analytical solution is a good estimation.

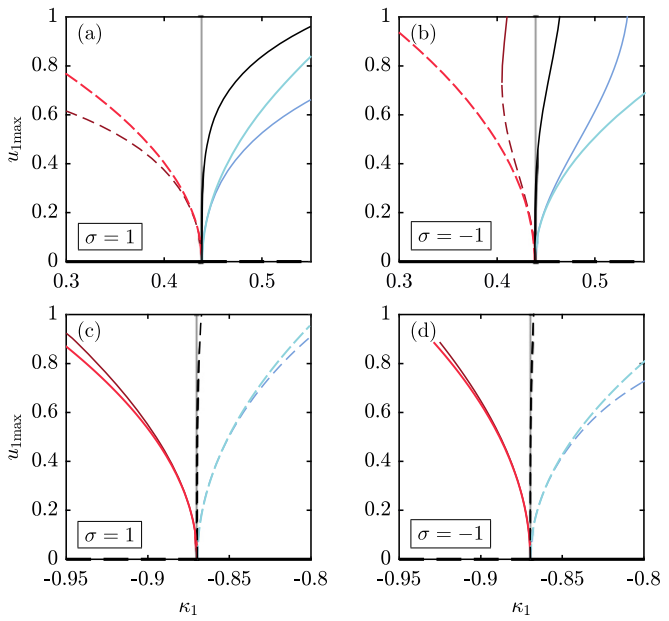

analytical	numerical	$\kappa_{\mathrm{nl},1}$ (a) $\kappa_{\mathrm{nl},1\mathrm{cr}}$	(b) $\kappa_{\mathrm{nl},1\mathrm{cr}}$	(c) $\kappa_{\mathrm{nl},1\mathrm{cr}}$	(d) $\kappa_{\mathrm{nl},1\mathrm{cr}}$
		0.015	0.025	0.0015	0.0005
		−0.025	−0.015	−0.0005	−0.0015

Fig. 4. Bifurcation diagrams of the collocated system also considering the nonlinear collocated control parameters. (a,b) with positive critical control parameter $\kappa_{1\mathrm{cr}} > 0$ and time delay $\tau = 0.1$; (c,d) with negative critical control parameter $\kappa_{1\mathrm{cr}} < 0$ and time delay $\tau = 0.8$. (a,c) with hardening stiffness nonlinearity ($\sigma = 1$); (b,d) with softening stiffness nonlinearity ($\sigma = -1$). The parameters are $r = 1$, $\gamma = 1$, $\chi = 0.05$. Darker and lighter colour sets show numerical and analytical results respectively. Continuous and dashed curves represent supercritical and subcritical branches respectively. The critical collocated control parameter $\kappa_{\mathrm{nl},1\mathrm{cr}}$ separates the subcritical and supercritical analytical results. The critical nonlinear control parameters can be found in Table 1. The table below the figure shows the investigated nonlinear collocated control parameters.

Table 1
Critical nonlinear collocated control parameters for the positive critical control parameter $\kappa_{1\mathrm{cr}} > 0$ with time delay $\tau = 0.1$ and negative critical control parameter $\kappa_{1\mathrm{cr}} < 0$ with time delay $\tau = 0.8$. The table shows the results with hardening ($\sigma = 1$) and softening ($\sigma = -1$) stiffness nonlinearity. The other parameters are $r = 1$, $\gamma = 1$, $\chi = 0.05$.

	$\tau = 0.1,\ \kappa_{1\mathrm{cr}} > 0$	$\tau = 0.8,\ \kappa_{1\mathrm{cr}} < 0$
$\sigma = 1$	$\kappa_{\mathrm{nl},1\mathrm{cr}} = -8.93 \cdot 10^{-3}$	$\kappa_{\mathrm{nl},1\mathrm{cr}} = 3.29 \cdot 10^{-4}$
$\sigma = -1$	$\kappa_{\mathrm{nl},1\mathrm{cr}} = 8.93 \cdot 10^{-3}$	$\kappa_{\mathrm{nl},1\mathrm{cr}} = -3.29 \cdot 10^{-4}$

5.1.2. Nonlinear control

In order to control the occurring Hopf bifurcation and make it supercritical, where it is actually subcritical due to the stiffness nonlinearity, we introduce the nonlinear collocated control parameter $\kappa_{\mathrm{nl},1}$. In this case, the Poincaré–Lyapunov constant takes the form

$$\Delta = C_{\kappa_{\mathrm{nl},1}} \kappa_{\mathrm{nl},1} + C_\sigma \sigma, \tag{55}$$

where $C_{\kappa_{\mathrm{nl},1}}$ and C_σ depend on the other parameters. The full formula is omitted in this study, because of its complexity. This simple formula shows a linear dependence on both the cubic nonlinear stiffness parameter σ and the nonlinear collocated control parameter $\kappa_{\mathrm{nl},1}$. For each parameter set a critical nonlinear collocated control parameter can be defined, when $\Delta = 0$ as

$$\kappa_{\mathrm{nl},1\mathrm{cr}} = -\frac{C_\sigma}{C_{\kappa_{\mathrm{nl},1}}} \sigma. \tag{56}$$

This critical nonlinear control parameter separates the local subcritical and supercritical analytical solutions near the critical bifurcation parameter. We assume that $C_{\kappa_{\mathrm{nl},1}} \neq 0$. The critical nonlinear collocated control $\kappa_{\mathrm{nl},1\mathrm{cr}}$ parameters for the parameter sets used in Fig. 4 can be found in Table 1. The values of the critical nonlinear control parameter $\kappa_{\mathrm{nl},1\mathrm{cr}}$ are symmetric for the hardening and softening nonlinearities, because of the linear dependence in (56). Bifurcation diagrams with numerical and analytical results for positive; negative critical control parameters ($\kappa_{1\mathrm{cr}} > 0$, $\kappa_{1\mathrm{cr}} < 0$) and hardening; softening nonlinearities ($\sigma = 1$, $\sigma = -1$) can be seen in Fig. 4 with several nonlinear control parameter values. It should be noted that it is not an easy task to initialize branches in the numerical continuation program for this particular system, which highlights the importance of the analytical solution. Although the analytical solution is only valid in the vicinity of the critical bifurcation parameter, it is easy to obtain results anywhere from the stability chart, once the analytical expressions are obtained, which is not true for the numerical solutions. The numerical results in Fig. 4 validate the analytical calculations. Near the critical bifurcation parameter, the analytical solutions are accurate. In Figs. 4(a,b) for $\kappa_{1\mathrm{cr}} > 0$, the analytical solutions become supercritical when $\kappa_{\mathrm{nl},1} < \kappa_{\mathrm{nl},1\mathrm{cr}}$. In contrast for Figs. 4(c,d) for $\kappa_{1\mathrm{cr}} < 0$ this condition is $\kappa_{\mathrm{nl},1} > \kappa_{\mathrm{nl},1\mathrm{cr}}$. The numerical results for $\kappa_{\mathrm{nl},1} = \kappa_{\mathrm{nl},1\mathrm{cr}}$ in Figs. 4(a,b) become supercritical after diverging from the analytical solution; Figs. 4(c,d) become slightly subcritical. In Fig. 4(b) the numerical result for $\kappa_{\mathrm{nl},1} = 0.015$ diverges from the analytical solution and becomes supercritical for higher amplitude values.

5.2. Non-collocated case

Now we investigate the non-collocated case, which means that the collocated control parameters are zero $\kappa_1 = 0$, $\kappa_{\mathrm{nl},1} = 0$.

5.2.1. Linear control

In this section we set the nonlinear control parameter to zero ($\kappa_{\mathrm{nl},2} = 0$). In Figs. 5(i) the value of the Poincaré–Lyapunov constant Δ is plotted against the time delay τ for (a) hardening stiffness nonlinearity $\sigma = 1$ and (b) softening stiffness nonlinearity $\sigma = -1$. In Figs. 5(ii) the bifurcations can be seen for a given parameter set for (a) positive critical control parameter $\kappa_{1\mathrm{cr}} > 0$ and (b) negative critical control parameter $\kappa_{1\mathrm{cr}} < 0$. The Poincaré–Lyapunov constant takes the same linear form as in (53)

$$\Delta = C_\sigma \sigma, \tag{57}$$

where C_σ depends on the other parameters and in this case can be written as in Eq. (58). Similarly to the collocated system with linear control investigated in Section 5.1.1, the bifurcations are subcritical ($\Delta > 0$) for hardening stiffness nonlinearity ($\sigma = 1$) and supercritical ($\Delta < 0$) for softening stiffness nonlinearity ($\sigma = -1$).

$$\begin{aligned} C_\sigma = {} & (3\omega^8(\omega^2-1)(-8\gamma^2\chi+\gamma^3(\tau-(r+1)\tau\omega^2)+\gamma\tau\omega^2(4\chi^2((r+1)\omega^2 \\ & -1)+\omega^2-1)+2\chi\omega^2(\omega^2+1))) \big/ (4\gamma(\gamma^4+2\gamma^2(2\chi^2-1)\omega^2+\omega^4) \\ & \times (\gamma^6(\tau^2\omega^2((r+1)\omega^2-1)^2+4)+2\gamma^4(4\chi^2\omega^2(\tau^2\omega^2((r+1)\omega^2-1)^2 \\ & +4)-\omega^4(\tau^2(\omega^2-1)((r+1)\omega^2-1)+4))+4\gamma^3\tau\chi\omega^4((r+1)\omega^4 \\ & -(r+6)\omega^2+3)+\gamma^2\omega^4(16\chi^4(\tau^2\omega^2((r+1)\omega^2-1)^2+4)-8\chi^2(\tau^2 \\ & \times(\omega^2-1)\omega^2((r+1)\omega^2-1)+4)+\tau^2\omega^2(\omega^2-1)^2+4\omega^4)+4\gamma\tau\chi \\ & \times\omega^6(4\chi^2((r+1)\omega^4+(r-2)\omega^2+1)-(\omega^2-1)^2)+4\chi^2\omega^6(\omega^2(\tau^2 \\ & \times(\omega^2-1)^2+\omega^2+2)+1))). \end{aligned} \tag{58}$$

5.2.2. Nonlinear control

With the introduction of the nonlinear non-collocated control parameter, we are able to control the bifurcations and change the subcritical behaviour to supercritical. The Poincaré–Lyapunov constant can be written in a similar form as in (55)

$$\Delta = C_{\kappa_{\mathrm{nl},2}} \kappa_{\mathrm{nl},2} + C_\sigma \sigma, \tag{59}$$

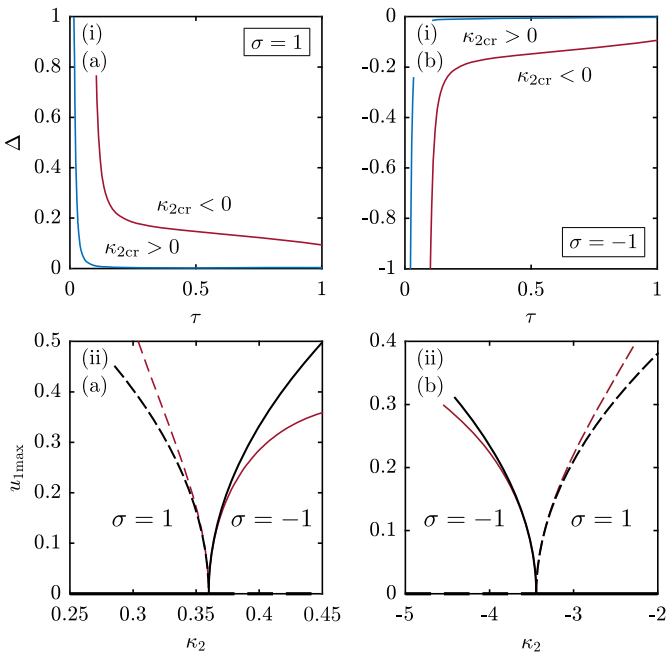

Fig. 5. (i) Poincaré–Lyapunov constant Δ of the non-collocated system against the time delay τ with linear collocated control for (a) hardening stiffness nonlinearity $\sigma = 1$; (b) softening stiffness nonlinearity $\sigma = -1$. The blue line represents the upper stability boundary, where the critical non-collocated control parameter is positive $\kappa_{2cr} > 0$ and the red line the lower stability boundary, where it is negative $\kappa_{2cr} < 0$. (ii) shows the bifurcations for (a) $\kappa_{2cr} > 0$ and (b) $\kappa_{2cr} < 0$. The black line represents the analytical solution and the red one the numerical result. The bifurcations are subcritical ($\Delta > 0$) for hardening stiffness nonlinearity ($\sigma = 1$) and supercritical ($\Delta < 0$) for softening stiffness nonlinearity ($\sigma = -1$). Continuous and dashed curves show supercritical and subcritical branches respectively. The parameters are $r = 1$, $\gamma = 1$, $\chi = 0.05$, $\tau = 0.15$. (For interpretation of the references to colour in this figure legend, the reader is referred to the web version of this article.)

where $C_{\kappa_{nl,2}}$ and C_σ depend on the other parameters. The full formula is omitted in this study, because of its complexity. A critical nonlinear non-collocated control parameter can be defined similarly to the collocated case in (56) as

$$\kappa_{nl,2cr} = -\frac{C_\sigma}{C_{\kappa_{nl,2}}}\sigma, \tag{60}$$

with $C_{\kappa_{nl,2}} \neq 0$. The critical nonlinear collocated control parameters for the parameter sets from Fig. 6 can be found in Table 2. Equation (60) is also linear; therefore, the critical nonlinear control parameter values are symmetric for the hardening ($\sigma = 1$) and softening ($\sigma = -1$) stiffness nonlinearities. It should be noted that these critical nonlinear control parameter values are 2–4 orders of magnitude larger than those of the collocated case in Table 1. This can also be an important aspect of the controller design. It is possible that the saturation of the controller prevents too large gains to be used. Also, producing larger gains requires more energy. Bifurcation diagrams with numerical and analytical results for positive; negative critical control parameters ($\kappa_{2cr} > 0$, $\kappa_{2cr} < 0$) and hardening; softening nonlinearities ($\sigma = 1$, $\sigma = -1$) can be seen in Fig. 6 with several nonlinear control parameter values. In Figs. 6(a,b) the analytical solutions become supercritical if $\kappa_{nl,2} < \kappa_{nl,2cr}$. Conversely, in Figs. 6(c,d) the bifurcations are supercritical if $\kappa_{nl,2} > \kappa_{nl,2cr}$. These conditions are similar to the conditions for the collocated case in Section 5.1.2. The numerical results for $\kappa_{nl,2} = \kappa_{nl,2cr}$ are supercritical after diverging from the analytical solution for all the investigated cases. In Fig. 6(b) the numerical result for $\kappa_{nl,2} = 2.7$ shows a strong supercritical behaviour after the initial subcritical branch, which is beneficial for the robustness. In Fig. 6(d) a similar behaviour can be seen for the parameter value $\kappa_{nl,2} = -20$.

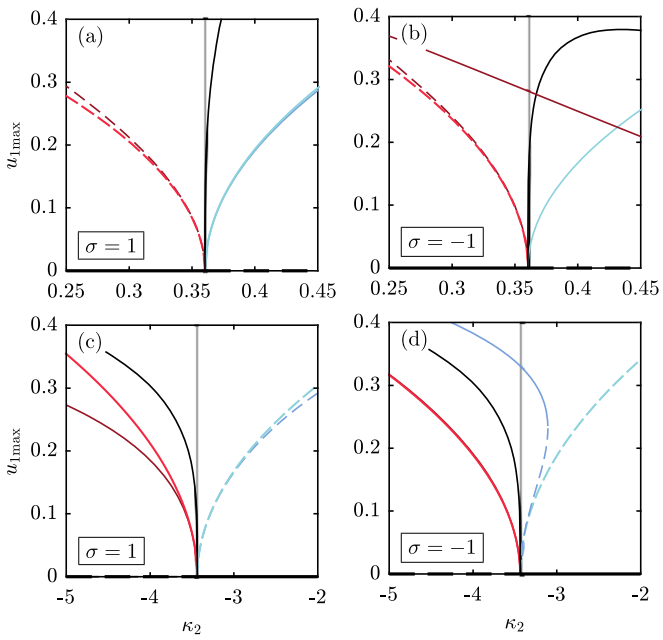

analytical	numerical	$\kappa_{nl,2}$ (a) $\kappa_{nl,2cr}$	(b) $\kappa_{nl,2cr}$	(c) $\kappa_{nl,2cr}$	(d) $\kappa_{nl,2cr}$
		2	2.7	20	5
		−2.7	−2	−5	−20

Fig. 6. Bifurcation diagrams of the non-collocated system also considering the nonlinear non-collocated control parameters. (a,b) with positive critical control parameter $\kappa_{2cr} > 0$; (c,d) with negative critical control parameter $\kappa_{2cr} < 0$. (a,c) with hardening stiffness nonlinearity ($\sigma = 1$); (b,d) with softening stiffness nonlinearity ($\sigma = -1$). The parameters are $r = 1$, $\gamma = 1$, $\chi = 0.05$, $\tau = 0.15$. Darker and lighter colour sets show numerical and analytical results respectively. Continuous and dashed curves represent supercritical and subcritical branches respectively. The critical non-collocated control parameter $\kappa_{nl,2cr}$ separates the subcritical and supercritical analytical results. The critical nonlinear control parameters can be found in Table 2. The table below the figure shows the investigated nonlinear non-collocated control $\kappa_{nl,2}$ parameter values.

Table 2
Critical nonlinear non-collocated control parameters for the positive critical control parameter $\kappa_{2cr} > 0$ and negative critical control parameter $\kappa_{2cr} < 0$ with time delay $\tau = 0.15$. The table shows the results with hardening ($\sigma = 1$) and softening ($\sigma = -1$) stiffness nonlinearity. The other parameters are $r = 1$, $\gamma = 1$, $\chi = 0.05$.

	$\tau = 0.15$, $\kappa_{2cr} > 0$	$\tau = 0.15$, $\kappa_{2cr} < 0$
$\sigma = 1$	$\kappa_{nl,2cr} = -6.87 \cdot 10^{-1}$	$\kappa_{nl,2cr} = 8.91$
$\sigma = -1$	$\kappa_{nl,2cr} = 6.87 \cdot 10^{-1}$	$\kappa_{nl,2cr} = -8.91$

6. General cubic stiffness nonlinearity

In this section, we add the second-order term to the nonlinear stiffness and analyse its effect on the Hopf bifurcations. With this term, the nonlinear stiffness represents realistic cases better and it is not an odd function anymore. Therefore, it is necessary to calculate the truncated form of $\mathbf{w}$ with Eqs. (39)–(47). The expressions can be obtained analytically in closed form. For hardening nonlinearity a condition can be derived, which ensures, that the nonlinear stiffness function does not turn back, which means that $k_{nl}(-\Delta x) < 0$ and $k_{nl}(\Delta x) > 0$. The condition can be written as

$$-2\gamma\sqrt{\sigma} \leq \nu \leq 2\gamma\sqrt{\sigma}. \tag{61}$$

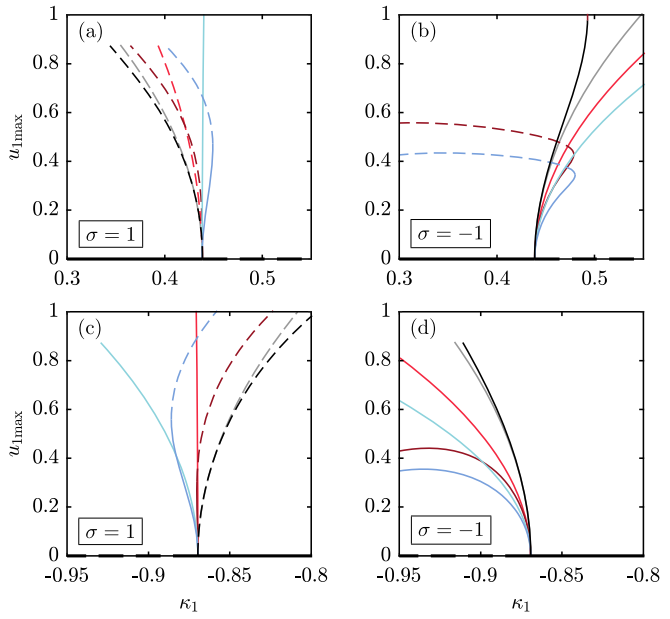

analytical	numerical	ν
		0
		1
		1.5

Fig. 7. Bifurcation diagrams of the collocated system with linear control considering the second-order term with coefficient ν. (a,b) with positive critical control parameter $\kappa_{1cr} > 0$ and time delay $\tau = 0.1$; (c,d) with negative critical control parameter $\kappa_{1cr} < 0$ and time delay $\tau = 0.8$. (a,c) with hardening stiffness nonlinearity $\sigma = 1$; (b,d) with softening stiffness nonlinearity $\sigma = -1$. The parameters are $r = 1$, $\gamma = 1$, $\chi = 0.05$. Darker and lighter colour sets show numerical and analytical results respectively. Continuous and dashed curves represent supercritical and subcritical branches respectively. The table shows the investigated second-order coefficient ν parameter values.

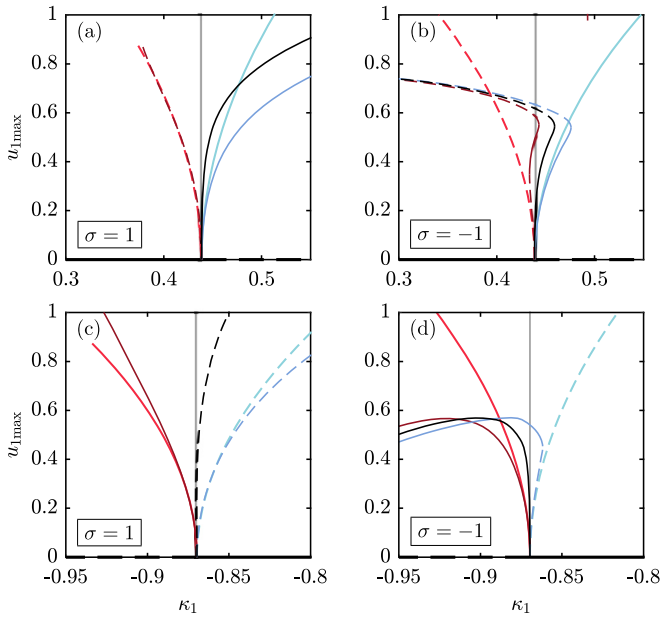

analytical	numerical	$\kappa_{\mathrm{nl},1}$ (a) $\kappa_{\mathrm{nl},1\mathrm{cr}}$	(b) $\kappa_{\mathrm{nl},1\mathrm{cr}}$	(c) $\kappa_{\mathrm{nl},1\mathrm{cr}}$	(d) $\kappa_{\mathrm{nl},1\mathrm{cr}}$
		−0.001	0.018	0.0007	−0.0001
		−0.014	0.001	−0.0002	−0.0007

Fig. 8. Bifurcation diagrams of the collocated system considering also the nonlinear collocated control parameters. (a,b) with positive critical control parameter $\kappa_{1cr} > 0$ and time delay $\tau = 0.1$; (c,d) with negative critical control parameter $\kappa_{2cr} < 0$ and time delay $\tau = 0.8$. (a,c) with hardening stiffness nonlinearity ($\sigma = 1$); (b,d) with softening stiffness nonlinearity ($\sigma = -1$). The parameters are $r = 1$, $\gamma = 1$, $\chi = 0.05$, $\nu = 0.5$. Darker and lighter colour sets show numerical and analytical results respectively. Continuous and dashed curves represent supercritical and subcritical branches respectively. The critical collocated control parameter $\kappa_{\mathrm{nl},1\mathrm{cr}}$ separates the subcritical and supercritical analytical results. The critical nonlinear control parameters can be found in Table 3. The table below the figure shows the investigated nonlinear collocated control parameter $\kappa_{\mathrm{nl},1}$ values.

6.1. Collocated case

Firstly, we analyse the collocated case, which means that the non-collocated control parameters are zero $\kappa_2 = 0$, $\kappa_{\mathrm{nl},2} = 0$.

6.1.1. Linear control

In this section, we analyse the collocated system without the nonlinear collocated control parameter ($\kappa_{\mathrm{nl},1} = 0$). The Poincaré–Lyapunov constant can be expressed in the form

$$\Delta = C_\sigma \sigma + C_\nu \nu^2, \tag{62}$$

where C_σ and C_ν depend on the other parameters. The full formula is omitted in this study, because of its complexity. It shows that the sign of ν is not important regarding the analytically calculated Hopf bifurcation. Therefore, only positive values of ν are considered. In Fig. 7 the bifurcations can be seen for a given parameter set for (a,b) positive critical control parameter $\kappa_{1cr} > 0$; (c,d) negative critical control parameter $\kappa_{1cr} < 0$. (a,c) shows the hardening stiffness nonlinearity ($\sigma = 1$); (b,d) softening stiffness nonlinearity ($\sigma = -1$). Generally, the second-order nonlinearity works towards supercriticality in the collocated system, which is beneficial from an engineering point of view. It makes the system more robust. In Fig. 7(a) the bifurcations for $\nu = 0$ and $\nu = 1$ are subcritical. With $\nu = 1.5$ the analytical solution gives slightly supercritical behaviour. However, the analytical solution becomes subcritical for higher amplitudes. In Fig. 7(b) the analytical solutions give supercritical behaviour for all the investigated ν parameters. The numerical results are subcritical after an initial supercritical branch. In Fig. 7(c) the bifurcation is subcritical for $\nu = 0$. The analytical solution for $\nu = 1$ gives slightly supercritical behaviour, but the numerical result is mainly subcritical. For $\nu = 1.5$, the analytical solution is already supercritical. However, the numerical result turns back and becomes subcritical. In Fig. 7(d) all the results are supercritical. The second-order nonlinearity strengthens the supercritical behaviour. However, one has to be careful, because the branches tend to become subcritical after an initial smaller supercritical branch.

Table 3
Critical nonlinear collocated control parameters for the positive critical control parameter $\kappa_{1cr} > 0$ with time delay $\tau = 0.1$ and negative critical control parameter $\kappa_{1cr} < 0$ with time delay $\tau = 0.8$. The table shows the results with hardening ($\sigma = 1$) and softening ($\sigma = -1$) stiffness nonlinearity. The other parameters are $r = 1$, $\gamma = 1$, $\chi = 0.05$, $\nu = 0.5$.

	$\tau = 0.1$, $\kappa_{1cr} > 0$	$\tau = 0.8$, $\kappa_{1cr} < 0$
$\sigma = 1$	$\kappa_{\mathrm{nl},1\mathrm{cr}} = -7.92 \cdot 10^{-3}$	$\kappa_{\mathrm{nl},1\mathrm{cr}} = 2.45 \cdot 10^{-4}$
$\sigma = -1$	$\kappa_{\mathrm{nl},1\mathrm{cr}} = 9.94 \cdot 10^{-3}$	$\kappa_{\mathrm{nl},1\mathrm{cr}} = -4.12 \cdot 10^{-4}$

6.1.2. Nonlinear control

We introduce the nonlinear collocated control parameter. The Poincaré–Lyapunov constant takes the form

$$\Delta = C_{\kappa_{\mathrm{nl},1}} \kappa_{\mathrm{nl},1} + C_\sigma \sigma + C_\nu \nu^2, \tag{63}$$

where $C_{\kappa_{\mathrm{nl},1}}$, C_σ and C_ν depend on the other parameters. The full formula is omitted in this study, because of its complexity. With this, the critical nonlinear collocated control parameter can be given in the

form

$$\kappa_{\mathrm{nl},1} = -\frac{C_\sigma}{C_{\kappa_{\mathrm{nl},1}}}\sigma - \frac{C_\nu}{C_{\kappa_{\mathrm{nl},1}}}\nu^2. \tag{64}$$

The critical nonlinear collocated control parameters for the parameter sets from Fig. 8 can be found in Table 3. Bifurcation diagrams with numerical and analytical results for positive; negative critical control parameters ($\kappa_{1\mathrm{cr}} > 0$, $\kappa_{1\mathrm{cr}} < 0$) and hardening; softening nonlinearities ($\sigma = 1$, $\sigma = -1$) can be seen in Fig. 8 for several nonlinear collocated control $\kappa_{\mathrm{nl},1}$ parameter values. In Figs. 8(a,b) the analytical solutions become supercritical if $\kappa_{\mathrm{nl},1} < \kappa_{\mathrm{nl},1\mathrm{cr}}$. Conversely, in Figs. 8(c,d) the bifurcations are supercritical if $\kappa_{\mathrm{nl},1} > \kappa_{\mathrm{nl},1\mathrm{cr}}$. In Figs. 8(a,d) the numerical results for $\kappa_{\mathrm{nl},1} = \kappa_{\mathrm{nl},1\mathrm{cr}}$ become supercritical after diverging from the analytical solution. In Fig. 8(c) it becomes subcritical. It is subcritical after an initial supercritical branch in Fig. 8(b). The numerical results in Fig. 8(b) become subcritical for higher amplitudes for all the investigated nonlinear control parameters, which is not favourable for robustness. Conversely in Fig. 8(d) the parameter values $\kappa_{\mathrm{nl},1} = \kappa_{\mathrm{nl},1\mathrm{cr}}$ and $\kappa_{\mathrm{nl},1} = -0.0001$ give strong supercritical behaviour. Furthermore, $\kappa_{\mathrm{nl},1} = -0.0007$ becomes strongly supercritical after a small subcritical branch. This means that for softening stiffness nonlinearity ($\sigma = -1$) from the viewpoint of robustness it is preferable to operate the controller in the negative stable region rather than in the positive.

6.2. Non-collocated case

Here we investigate the non-collocated case, which means that the collocated control parameters are zero $\kappa_1 = 0$, $\kappa_{\mathrm{nl},1} = 0$.

6.2.1. Linear control

In this section, we analyse the non-collocated system without the nonlinear non-collocated control parameter ($\kappa_{\mathrm{nl},2} = 0$). The Poincaré–Lyapunov can be expressed in the same form as in (62)

$$\Delta = C_\sigma \sigma + C_\nu \nu^2, \tag{65}$$

where C_σ and C_ν depend on the other parameters. The full formula is omitted in this study, because of its complexity. In Fig. 9 the bifurcations can be seen for a given parameter set for (a,b) positive critical control parameter $\kappa_{2\mathrm{cr}} > 0$; (c,d) negative critical control parameter $\kappa_{2\mathrm{cr}} < 0$. (a,c) shows the hardening stiffness nonlinearity ($\sigma = 1$); (b,d) softening stiffness nonlinearity ($\sigma = -1$). Generally, the second-order nonlinearity tends to make the bifurcations more supercritical, similarly to the collocated case. In Fig. 9(a) the bifurcation is slightly subcritical for $\nu = 0$ and becomes supercritical for the other investigated ν values. In Fig. 9(b) all the bifurcations are supercritical and larger ν values strengthen this property. In Fig. 9(c) the bifurcations are subcritical with $\nu = 0$ and $\nu = 1$. Furthermore, the bifurcation with the analytical solution for $\nu = 1.5$ is also subcritical. In contrast, the numerical result for this parameter value shows a rather strong supercritical behaviour. In this case, the analytical and numerical results are quite different. Possibly, the region, where the analytical solution gives a good approximation is very small. In Fig. 9(d) all the bifurcations are supercritical with the investigated parameters and larger ν values decrease the amplitude of the supercritical branch.

6.2.2. Nonlinear control

We introduce the nonlinear non-collocated control parameter. in order to control the occurring Hopf bifurcations. The Poincaré–Lyapunov can be written in a similar form as in (63).

$$\Delta = C_{\kappa_{\mathrm{nl},2}}\kappa_{\mathrm{nl},2} + C_\sigma \sigma + C_\nu \nu^2. \tag{66}$$

where $C_{\kappa_{\mathrm{nl},2}}$, C_σ and C_ν depend on the other parameters. The full formula is omitted in this study, because of its complexity. The critical

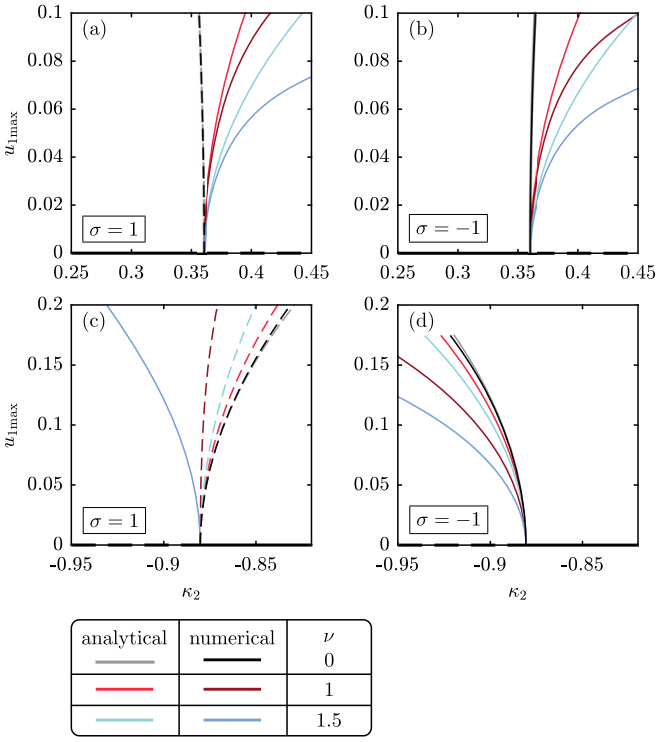

Fig. 9. Bifurcation diagrams of the non-collocated system with linear control considering the second-order term with coefficient ν. (a,b) with positive critical control parameter $\kappa_{2\mathrm{cr}} > 0$ and time delay $\tau = 0.15$; (c,d) with negative critical control parameter $\kappa_{2\mathrm{cr}} < 0$ and time delay $\tau = 0.3$. (a,c) with hardening stiffness nonlinearity $\sigma = 1$; (b,d) with softening stiffness nonlinearity $\sigma = -1$. The parameters are $r = 1$, $\gamma = 1$, $\chi = 0.05$. Darker and lighter colour sets show numerical and analytical results respectively. Continuous and dashed curves represent supercritical and subcritical branches respectively. The table shows the investigated second-order coefficient ν parameter values.

nonlinear non-collocated control parameter can be defined similarly to the collocated case in (64) as

$$\kappa_{\mathrm{nl},2\mathrm{cr}} = -\frac{C_\sigma}{C_{\kappa_{\mathrm{nl},2}}}\sigma - \frac{C_\nu}{C_{\kappa_{\mathrm{nl},2}}}\nu^2. \tag{67}$$

The critical nonlinear non-collocated control parameters for the parameter sets from Fig. 10 can be found in Table 4. Bifurcation diagrams with numerical and analytical results for positive; negative critical control parameters ($\kappa_{1\mathrm{cr}} > 0$, $\kappa_{1\mathrm{cr}} < 0$) and hardening; softening nonlinearities ($\sigma = 1$, $\sigma = -1$) can be seen in Fig. 10. The bifurcations were plotted for several nonlinear non-collocated control parameters. The conditions of supercriticality of the analytical solution are $\kappa_{\mathrm{nl},2} < \kappa_{\mathrm{nl},2\mathrm{cr}}$ for Figs. 10(a,b) and $\kappa_{\mathrm{nl},2} > \kappa_{\mathrm{nl},2\mathrm{cr}}$ for Figs. 10(c,d). In all investigated bifurcations the numerical result for $\kappa_{\mathrm{nl},2} = \kappa_{\mathrm{nl},2\mathrm{cr}}$ is supercritical after diverging from the analytical solution. In Fig. 10(b) the results for the nonlinear control parameters $\kappa_{\mathrm{nl},2} = \kappa_{\mathrm{nl},2\mathrm{cr}}$ and $\kappa_{\mathrm{nl},2} = 7$ show strong higher-order properties. In Fig. 10(d) the results of the analytical and numerical solutions with $\kappa_{\mathrm{nl},2} = 0.5$ are very close to each other in the investigated amplitude region, there is practically no difference between the two curves in the figure.

7. Conclusions

The main focus of this study was to give a detailed general derivation of the Hopf bifurcation calculation in neutral delay differential equations using the centre manifold reduction and Poincaré normal

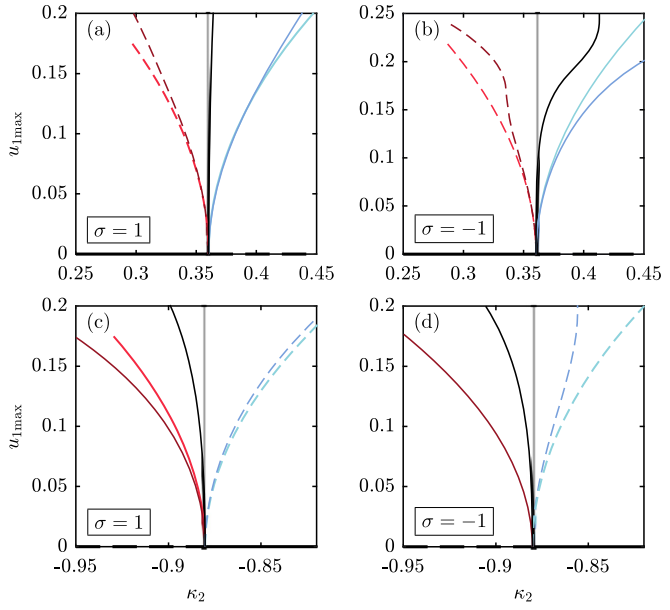

analytical	numerical	$\kappa_{\mathrm{nl},2}$ (a) $\kappa_{\mathrm{nl},2\mathrm{cr}}$	(b) $\kappa_{\mathrm{nl},2\mathrm{cr}}$	(c) $\kappa_{\mathrm{nl},2\mathrm{cr}}$	(d) $\kappa_{\mathrm{nl},2\mathrm{cr}}$
		5	7	2.5	0.5
		−3	−2	−0.5	−2.5

Fig. 10. Bifurcation diagrams of the non-collocated system with different nonlinear non-collocated control parameters and hardening $\sigma = 1$; softening $\sigma = -1$ nonlinearities for the parameter values $r = 1$, $\gamma = 1$, $\chi = 0.05$, $\nu = 0.5$. The Hopf bifurcation (a,b) for positive critical control parameters $\kappa_{2\mathrm{cr}} > 0$ and time delay $\tau = 0.15$; (c,d) for negative critical control parameters $\kappa_{2\mathrm{cr}} < 0$ and time delay $\tau = 0.3$. Darker and lighter colour sets show numerical and analytical results respectively. Continuous and dashed curves represent supercritical and subcritical branches respectively. The critical collocated control parameter $\kappa_{\mathrm{nl},2\mathrm{cr}}$ separates the subcritical and supercritical analytical results. The critical nonlinear control parameters can be found in Table 4. The table below the figure shows the investigated nonlinear non-collocated control parameter $\kappa_{\mathrm{nl},2}$ values.

form. This derivation was presented in Section 4. The problem was inspired by industrial robotic machining when the measured acceleration of the end effector is fed back to the dedicated position control of the robot. The work is dealing with analysing the underlying stiffening nonlinear behaviour of an industrial robot. The realized control was developed to ensure the local stability of the robotic arm before actually performing the machining operation, which results in a high dimensional neutral type of nonlinear equation. The nonlinear stiffness of the robotic arm was modelled with a third-order polynomial function. The adopted two degrees-of-freedom mathematical model was described in detail in Section 2. Two different configurations were distinguished depending on the location of the acceleration sensor. The collocated case represents a robotic arm with the acceleration sensor close to the actuator and the non-collocated case with the sensor near the end effector. All analytical results were validated by numerical solutions obtained with the NDDE-cont continuation software. This showed that the analytical calculations give a good local approximation of the nonlinear behaviour in the vicinity of the critical bifurcation parameter.

At first, the second-order term in the stiffness characteristic was neglected in Section 5. The third order-term was considered to model

Table 4
Critical nonlinear non-collocated control parameters for the positive critical control parameter $\kappa_{2\mathrm{cr}} > 0$ with time delay $\tau = 0.15$ and negative critical control parameter $\kappa_{2\mathrm{cr}} < 0$ with time delay $\tau = 0.3$. The table shows the results with hardening ($\sigma = 1$) and softening ($\sigma = -1$) stiffness nonlinearity. The other parameters are $r = 1$, $\gamma = 1$, $\chi = 0.05$, $\nu = 0.5$.

	$\tau = 0.15$, $\kappa_{2\mathrm{cr}} > 0$	$\tau = 0.3$, $\kappa_{2\mathrm{cr}} < 0$
$\sigma = 1$	$\kappa_{\mathrm{nl},2\mathrm{cr}} = 1.12$	$\kappa_{\mathrm{nl},2\mathrm{cr}} = 1.07$
$\sigma = -1$	$\kappa_{\mathrm{nl},2\mathrm{cr}} = 2.49$	$\kappa_{\mathrm{nl},2\mathrm{cr}} = -1.18$

the main nonlinear stiffness of industrial robotic arms. The Hopf bifurcation was calculated first considering only a linear acceleration feedback controller. The systems with hardening and softening stiffness nonlinearities showed different behaviours. Namely, the bifurcations were supercritical for softening nonlinearity and subcritical for hardening nonlinearity. In order to modify the possible subcritical behaviour of the system, which can limit robustness, we introduced a third-order nonlinear term in the acceleration control law. With this nonlinear controller, we were able to define a critical nonlinear control parameter, which divides the sub- and supercritical analytical solutions. Whether to use the collocated or the non-collocated setup is up to the specific parameters of the system. However, we would like to note that in the non-collocated case much larger nonlinear gains are needed to modify the subcritical bifurcations compared to the collocated case. Furthermore, in the collocated case with non-symmetric stiffness nonlinearity, the bifurcations tend to become subcritical after an initial supercritical branch, which limits robustness. In these cases, it may be advisable to use the non-collocated setup. In the other cases also the results should be checked with the numerical continuation to find these fold bifurcations. If it is present maybe the other setup can provide sufficiently robust results.

From the presented results, clear suggestions can be made to improve the robustness of the system by modifying the occurring subcritical bifurcations to supercritical ones. These results were also studied with numerical continuation, which showed that results far from the critical bifurcation parameters can diverge from the locally valid analytical results. This highlights the importance of also analysing the global dynamic behaviour, as it can still limit robustness and the effectiveness of the utilized acceleration controller.

With the introduction of the second-order term in the stiffness characteristic in Section 6, we also investigated the non-symmetric behaviour of the stiffness. The analytical results showed that the sign of the second-order term does not change the bifurcations of the system, only its magnitude is important. In the vicinity of the critical bifurcation parameter, the second-order term works toward supercritical behaviour in both the collocated and non-collocated cases. This is beneficial from an engineering point of view because it improves robustness and works towards safety. We also carried out the same procedure as in Section 5 namely, introduced the nonlinear control parameters and defining the critical values that divide sub- and supercritical behaviour near the critical bifurcation parameter. However, the numerical results showed that the bifurcations, especially in the collocated case can become subcritical after an initial supercritical branch diverging from the analytical solution. Although the analytical solution showed supercriticality near the critical bifurcation parameter, this behaviour can still limit robustness and one has to be careful of the global dynamic picture in the development of nonlinear controllers.

In summary, the analytical expressions from the Hopf bifurcation calculation of neutral delay differential equations were successfully validated with the NDDE-cont numerical continuation software. With the obtained analytical results, we were able to design a nonlinear controller to modify the unfavourable nonlinear properties of the system. Although the analytical solutions gave a good approximation of

the local nonlinear behaviour, near the critical bifurcation parameter, these results should always be analysed together with numerical results, which provide information about the global dynamic behaviour as well. The analytical calculations gave a good basis for analysing and developing nonlinear controllers, as they can provide analytical closed-form solutions, but one should always be weary of the global dynamic behaviour as well.

CRediT authorship contribution statement

Andras Bartfai: Conceptualization, Methodology, Software, Validation, Formal analysis, Investigation, Resources, Data curation, Writing – original draft, Writing – review & editing, Visualization. **Zoltan Dombovari:** Conceptualization, Methodology, Formal analysis, Resources, Writing – review & editing, Supervision, Project administration, Funding acquisition.

Declaration of competing interest

The authors declare that they have no known competing financial interests or personal relationships that could have appeared to influence the work reported in this paper.

Acknowledgement

This research was supported by the National Research, Development and Innovation Office of the Hungarian Government in the framework of the NKFI FK 124361 research project.

Appendix A. Derivation of the bilinear form for the neutral case

Here, we provide the detailed derivation of the bilinear form for the neutral case. The general bilinear form a can be found in [26]. In this study, we aim to derive the bilinear form for the neutral case in a simpler form. We refer to [29], where it was derived from the usual inner product for the retarded case as

$$\langle \mathbf{u}(\vartheta), \mathbf{v}(\vartheta)\rangle = \int_{-\tau}^{0} \mathbf{u}^{\mathsf{H}}(\vartheta+\tau)\,\mathbf{R}\,\mathbf{v}(\vartheta)\,\mathrm{d}\vartheta + \mathbf{u}^{\mathsf{H}}(0)\,\mathbf{v}(0). \tag{A.1}$$

Modifying (A.1) for the neutral case. Instinctively, we assume that the derivative term $\mathbf{v}'$ is acting in (A.1) for the neutral case

$$\langle \mathbf{u}(\vartheta), \mathbf{v}(\vartheta)\rangle = \int_{-\tau}^{0} \mathbf{u}^{\mathsf{H}}(\vartheta+\tau)\,\mathbf{R}\,\mathbf{v}'(\vartheta)\,\mathrm{d}\vartheta + \mathbf{u}^{\mathsf{H}}(0)\,\mathbf{v}(0). \tag{A.2}$$

Applying the defined bilinear form on $\mathscr{A}\mathbf{v}$ gives

$$\begin{aligned}
\langle \mathbf{u}(\vartheta), \mathscr{A}\mathbf{v}(\vartheta)\rangle &= \int_{-\tau}^{0} \mathbf{u}^{\mathsf{H}}(\vartheta+\tau)\,\mathbf{R}\,\mathbf{v}''(\vartheta)\,\mathrm{d}\vartheta + \mathbf{u}^{\mathsf{H}}(0)\,(\mathbf{L}\,\mathbf{v}(0) + \mathbf{R}\,\mathbf{v}(-\tau)) \\
&= -\int_{-\tau}^{0} \mathbf{u}'^{\mathsf{H}}(\vartheta+\tau)\,\mathbf{R}\,\mathbf{v}'(\vartheta)\,\mathrm{d}\vartheta + \left[\mathbf{u}^{\mathsf{H}}(\vartheta+\tau)\,\mathbf{R}\,\mathbf{v}'(\vartheta)\right]_{-\tau}^{0} + \mathbf{u}^{\mathsf{H}}(0)\,\mathbf{L}\,\mathbf{v}(0) \\
&\quad + \mathbf{u}^{\mathsf{H}}(0)\,\mathbf{R}\,\mathbf{v}(-\tau) \\
&= -\int_{-\tau}^{0} \mathbf{u}'^{\mathsf{H}}(\vartheta+\tau)\,\mathbf{R}\,\mathbf{v}'(\vartheta)\,\mathrm{d}\vartheta + \mathbf{u}^{\mathsf{H}}(0)\,\mathbf{L}\,\mathbf{v}(0) + \mathbf{u}^{\mathsf{H}}(\tau)\,\mathbf{R}\,\mathbf{v}'(0) \\
&= -\int_{-\tau}^{0} \mathbf{u}'^{\mathsf{H}}(\vartheta+\tau)\,\mathbf{R}\,\mathbf{v}'(\vartheta)\,\mathrm{d}\vartheta + \mathbf{u}^{\mathsf{H}}(0)\,\mathbf{L}\,\mathbf{v}(0) + \mathbf{u}^{\mathsf{H}}(\tau)\,\mathbf{R}\,(\mathbf{L}\,\mathbf{v}(0) + \mathbf{R}\,\mathbf{v}'(-\tau)).
\end{aligned} \tag{A.3}$$

It can be seen that in this form $\mathscr{A}^*$ cannot be given to satisfy the formal adjoint problem in (29). By getting rid of the terms that have mixed product of $\mathbf{L}$ and $\mathbf{R}$ and second order product with $\mathbf{R}$, the bilinear form can be modified as

$$\langle \mathbf{u}(\vartheta), \mathbf{v}(\vartheta)\rangle = \int_{-\tau}^{0} \mathbf{u}^{\mathsf{H}}(\vartheta+\tau)\,\mathbf{R}\,\mathbf{v}'(\vartheta)\,\mathrm{d}\vartheta + (\mathbf{u}^{\mathsf{H}}(0) - \mathbf{u}^{\mathsf{H}}(\tau)\,\mathbf{R})\,\mathbf{v}(0) \tag{A.4}$$

similarly as in [33,34] for scalar neutral equations. This is the bilinear form for the neutral case. With this form the expression with operator $\mathscr{A}$, following the same steps as in (A.3), reduces to

$$\langle \mathbf{u}(\vartheta), \mathscr{A}\mathbf{v}(\vartheta)\rangle = -\int_{-\tau}^{0} \mathbf{u}'^{\mathsf{H}}(\vartheta+\tau)\,\mathbf{R}\,\mathbf{v}'(\vartheta)\,\mathrm{d}\vartheta + \mathbf{u}^{\mathsf{H}}(0)\,\mathbf{L}\,\mathbf{v}(0). \tag{A.5}$$

Naturally, the adjoint operator $\mathscr{A}^*$ satisfies the formal adjoint problem with the bilinear form for the neutral case

$$\langle \mathscr{A}^*\mathbf{u}(\vartheta), \mathbf{v}(\vartheta)\rangle = \langle \mathbf{u}(\vartheta), \mathscr{A}\mathbf{v}(\vartheta)\rangle = -\int_{-\tau}^{0} \mathbf{u}'^{\mathsf{H}}(\vartheta+\tau)\,\mathbf{R}\,\mathbf{v}'(\vartheta)\,\mathrm{d}\vartheta + \mathbf{u}^{\mathsf{H}}(0)\,\mathbf{L}\,\mathbf{v}(0). \tag{A.6}$$

Appendix B. Decomposition of the solution at the centre subspace

The solution $\mathbf{u}_t(\vartheta)$ can be decomposed into the components $z_{1,2} : \mathbb{R} \to \mathbb{R}$ tangent to the centre subspace and into the infinite-dimensional component $\mathbf{w} : \mathbb{R} \to \mathbb{X}_{\mathbb{R}^n}$ transverse to the centre subspace

$$\mathbf{u}_t(\vartheta) = z_1(t)\,\mathbf{s}_{\mathrm{R}}(\vartheta) + z_2(t)\,\mathbf{s}_{\mathrm{I}}(\vartheta) + \mathbf{w}(t)(\vartheta), \tag{B.1}$$

where

$$\begin{aligned}
z_1(t) &= \langle \mathbf{n}_{\mathrm{R}},\ \mathbf{u}_t\rangle, \\
z_2(t) &= \langle \mathbf{n}_{\mathrm{I}},\ \mathbf{u}_t\rangle, \\
\mathbf{w}(t) &= \mathbf{u}_t - z_1(t)\,\mathbf{s}_{\mathrm{R}} - z_2(t)\,\mathbf{s}_{\mathrm{I}}.
\end{aligned} \tag{B.2}$$

Taking the derivative of the new variables with respect to time gives

$$\begin{aligned}
\dot{z}_1(t) &= \langle \mathbf{n}_{\mathrm{R}},\ \dot{\mathbf{u}}_t\rangle = \omega\, z_2 + \mathbf{n}_{\mathrm{R}}^{\mathsf{T}}(0)\,\mathbf{F} = \omega\, z_2 + \mathbf{N}_1^{\mathsf{T}}\mathbf{F}, \\
\dot{z}_2(t) &= \langle \mathbf{n}_{\mathrm{I}},\ \dot{\mathbf{u}}_t\rangle = -\omega\, z_1 + \mathbf{n}_{\mathrm{I}}^{\mathsf{T}}(0)\,\mathbf{F} = -\omega\, z_1 + \mathbf{N}_2^{\mathsf{T}}\mathbf{F}, \\
\dot{\mathbf{w}}(t) &= \dot{\mathbf{u}}_t - \dot{z}_1\mathbf{s}_{\mathrm{R}} - \dot{z}_2\mathbf{s}_{\mathrm{I}} = \mathscr{A}\mathbf{w} + \mathscr{F}(\mathbf{u}_t) - \mathbf{n}_{\mathrm{R}}^{\mathsf{T}}(0)\,\mathbf{F}\,\mathbf{s}_{\mathrm{R}} - \mathbf{n}_{\mathrm{I}}^{\mathsf{T}}(0)\,\mathbf{F}\,\mathbf{s}_{\mathrm{I}} \\
&\quad = \mathscr{A}\mathbf{w} + \mathscr{F}(\mathbf{u}_t) - \mathbf{N}_1^{\mathsf{T}}\mathbf{F}\,\mathbf{s}_{\mathrm{R}} - \mathbf{N}_2^{\mathsf{T}}\mathbf{F}\,\mathbf{s}_{\mathrm{I}},
\end{aligned} \tag{B.3}$$

where $\mathbf{F} = \mathscr{F}(z_1(t)\,\mathbf{s}_{\mathrm{R}} + z_2(t)\,\mathbf{s}_{\mathrm{I}} + \mathbf{w}(t))\,(0)$. For the detailed calculation see [29]. Writing it into matrix form yields

$$\begin{bmatrix} \dot{z}_1 \\ \dot{z}_2 \\ \dot{\mathbf{w}} \end{bmatrix} = \begin{bmatrix} 0 & \omega & 0 \\ -\omega & 0 & 0 \\ 0 & 0 & \mathscr{A} \end{bmatrix} \begin{bmatrix} z_1 \\ z_2 \\ \mathbf{w} \end{bmatrix} + \begin{bmatrix} \mathbf{N}_1^{\mathsf{T}}\mathbf{F} \\ \mathbf{N}_2^{\mathsf{T}}\mathbf{F} \\ \mathscr{F}(\mathbf{u}_t) - \mathbf{N}_1^{\mathsf{T}}\mathbf{F}\,\mathbf{s}_{\mathrm{R}} - \mathbf{N}_2^{\mathsf{T}}\mathbf{F}\,\mathbf{s}_{\mathrm{I}} \end{bmatrix}. \tag{B.4}$$

For the Hopf bifurcation, the nonlinear terms in z_1 and z_2 should be expanded with Taylor series up to third order and in $\mathbf{w}$ up to second-order terms. This gives

$$\begin{aligned}
\begin{bmatrix} \dot{z}_1 \\ \dot{z}_2 \\ \dot{\mathbf{w}} \end{bmatrix} &= \begin{bmatrix} 0 & \omega & 0 \\ -\omega & 0 & 0 \\ 0 & 0 & \mathscr{A} \end{bmatrix} \begin{bmatrix} z_1 \\ z_2 \\ \mathbf{w} \end{bmatrix} + \begin{bmatrix} \sum_{j,k\geq 0}^{j+k=2,3} f_{jk0}^{(1)} z_1^j z_2^k \\ \sum_{j,k\geq 0}^{j+k=2,3} f_{jk0}^{(2)} z_1^j z_2^k \\ \sum_{j,k\geq 0}^{j+k=2} \left(\mathbf{f}_{jk0}^{(3c)} \cos\omega\vartheta + \mathbf{f}_{jk0}^{(3s)} \sin\omega\vartheta\right) z_1^j z_2^k \end{bmatrix} \\
&\quad + \begin{bmatrix} \sum_{i=1}^{n} \left(f_{101,i}^{(10)} z_1 + f_{011,i}^{(10)} z_2\right) w_i(0) + \left(f_{101,i}^{(1\tau)} z_1 + f_{011,i}^{(1\tau)} z_2\right) w_i'(-\tau) \\ \sum_{i=1}^{n} \left(f_{101,i}^{(20)} z_1 + f_{011,i}^{(20)} z_2\right) w_i(0) + \left(f_{101,i}^{(2\tau)} z_1 + f_{011,i}^{(2\tau)} z_2\right) w_i'(-\tau) \\ \begin{cases} \mathbf{0}, & \vartheta \in [-\tau, 0), \\ \sum_{j,k\geq 0}^{j+k=2} \mathbf{f}_{jk0}^{(3)}, & \vartheta = 0 \end{cases} \end{bmatrix},
\end{aligned} \tag{B.5}$$

where

$$\begin{aligned}
f_{jk0}^{(1)} &= \frac{1}{j!k!} \left.\frac{\partial^{j+k}\mathbf{N}_1^{\mathsf{T}}\mathbf{F}}{\partial z_1^j \partial z_2^k}\right|_{\mathbf{0}}, \qquad f_{jkm,i}^{(10)} = \frac{1}{j!k!m!} \left.\frac{\partial^{j+k+m}\mathbf{N}_1^{\mathsf{T}}\mathbf{F}}{\partial z_1^j \partial z_2^k \partial w_i^m(0)}\right|_{\mathbf{0}}, \\
f_{jkm,i}^{(1\tau)} &= \frac{1}{j!k!m!} \left.\frac{\partial^{j+k+m}\mathbf{N}_1^{\mathsf{T}}\mathbf{F}}{\partial z_1^j \partial z_2^k \partial w_i'^m(-\tau)}\right|_{\mathbf{0}}, \\
f_{jk0}^{(2)} &= \frac{1}{j!k!} \left.\frac{\partial^{j+k}\mathbf{N}_2^{\mathsf{T}}\mathbf{F}}{\partial z_1^j \partial z_2^k}\right|_{\mathbf{0}}, \qquad f_{jkm,i}^{(20)} = \frac{1}{j!k!m!} \left.\frac{\partial^{j+k+m}\mathbf{N}_2^{\mathsf{T}}\mathbf{F}}{\partial z_1^j \partial z_2^k \partial w_i^m(0)}\right|_{\mathbf{0}}, \\
f_{jkm,i}^{(2\tau)} &= \frac{1}{j!k!m!} \left.\frac{\partial^{j+k+m}\mathbf{N}_2^{\mathsf{T}}\mathbf{F}}{\partial z_1^j \partial z_2^k \partial w_i'^m(-\tau)}\right|_{\mathbf{0}}
\end{aligned} \tag{B.6}$$

are real constant coefficients and

$$\mathbf{f}_{jk0}^{(3c)} = [\cos\omega\vartheta]\left(\frac{1}{j!k!}\left.\frac{\partial^{j+k}(-\mathbf{N}_1^{\mathsf{T}}\mathbf{F}\,\mathbf{s}_{\mathrm{R}} - \mathbf{N}_2^{\mathsf{T}}\mathbf{F}\,\mathbf{s}_{\mathrm{I}})}{\partial z_1^j \partial z_2^k}\right|_{\mathbf{0}}\right),$$
$$\mathbf{f}_{jk0}^{(3s)} = [\sin\omega\vartheta]\left(\frac{1}{j!k!}\left.\frac{\partial^{j+k}(-\mathbf{N}_1^{\mathsf{T}}\mathbf{F}\,\mathbf{s}_{\mathrm{R}} - \mathbf{N}_2^{\mathsf{T}}\mathbf{F}\,\mathbf{s}_{\mathrm{I}})}{\partial z_1^j \partial z_2^k}\right|_{\mathbf{0}}\right), \tag{B.7}$$
$$\mathbf{f}_{jk0}^{(3)} = \frac{1}{j!k!}\left.\frac{\partial^{j+k}\mathbf{F}}{\partial z_1^j \partial z_2^k}\right|_{\mathbf{0}}$$

are real vector coefficients. The notations $[\cos\omega\vartheta]$ and $[\sin\omega\vartheta]$ mean the coefficient of $\cos\omega\vartheta$ and $\sin\omega\vartheta$ respectively. We note here that for nonlinearities of odd functions, the calculation of $\mathbf{w}$ is not necessary, since in this case the coefficients of the mixed terms with $z_{1,2}$ and w_i become zero. In the Taylor expansion, the coefficients from even order derivatives are always zero. This means that the first two rows in (B.5) can be separated and the approximate periodic solution can be directly calculated by expanding only the nonlinearities of $\dot{z}_1$ and $\dot{z}_2$ up to third-degree. We can also notice that for odd functions, the vector coefficients in (B.7) become zero vectors.

References

[1] A. Verl, A. Valente, S. Melkote, C. Brecher, E. Ozturk, T.T. Lutfi, Robots in machining, CIRP Ann. 68 (2) (2019) 799–822.

[2] E. Ozturk, A. Barrios, C. Sun, S. Rajabi, J. Munoa, Robotic assisted milling for increased productivity, CIRP Ann. 67 (1) (2018) 427–430.

[3] T. Insperger, G. Stépán, Stability of the milling process, Period. Polytech. Mech. Eng. 44 (1) (2000) 47–57.

[4] G. Stépán, T. Kalmár-Nagy, Nonlinear regenerative machine tool vibrations, in: Proceedings of the ASME 1997 Design Engineering Technical Conferences, 1, ASME, 1997.

[5] G. Stépán, Modelling nonlinear regenerative effects in metal cutting, Phil. Trans. R. Soc. A 359 (1781) (2001) 739–757.

[6] G. Stépán, R. Szalai, T. Insperger, Nonlinear Dynamics of High-Speed Milling Subjected to Regenerative Effect, John Wiley & Sons, Ltd, 2004, pp. 111–128.

[7] B. Ermentrout, Simulating, Analyzing, and Animating Dynamical Systems: A Guide to XPPAUT for Researchers and Students, Vol. 14, Society for Industrial and Applied Mathematics (SIAM), 2002.

[8] E.J. Doedel, A.R. Champneys, T.F. Fairgrieve, Y.A. Kuznetsov, B. Sandstede, X. Wang, AUTO97–AUTO2000: Continuation and bifurcation software for ordinary differential equations (with HomCont), in: User's Guide, Concordia University, Montreal, Canada, 2001, pp. 1997–2000.

[9] A. Back, J. Guckenheimer, M. Myers, F. Wicklin, P. Worfolk, DsTool: Computer assisted exploration of dynamical systems, AMS Notices 39 (1995) 303–309.

[10] R. Clewley, Hybrid models and biological model reduction with PyDSTool, PLoS Comput. Biol. 8 (8) (2012).

[11] A.I. Khibnik, Y.A. Kuznetsov, V.V. Levitin, E.V. Nikolaev, LOCBIF: Interactive Local Bifurcation Analyser, Version 2, Russian Academy of Sciences, Institute of Mathematical Problems in Biology, 1993.

[12] A. Dhooge, W. Govaerts, Y.A. Kuznetsov, MATCONT: A MATLAB package for numerical bifurcation analysis of ODEs, ACM Trans. Math. Software 29 (2) (2003) 141–164.

[13] Y.A. Kuznetsov, V.V. Levitin, Integrated environment for analysis of dynamical systems, 1997, CWI, Amsterdam, Available via anonymous ftp from ftp://ftp.cwi.nl/pub/CONTENT.

[14] H. Dankowicz, F. Schilder, Recipes for Continuation, in: Computational Science and Engineering, vol. 11, Society for Industrial and Applied Mathematics (SIAM), 2013.

[15] G. Stepan, Retarded Dynamical Systems: Stability and Characteristic Functions, in: Pitman Research Notes in Mathematics Series, Longman Science & Technology, 1990.

[16] K. Engelborghs, T. Luzyanina, G. Samaey, DDE-BIFTOOL: A matlab package for bifurcation analysis of delay differential equations, TW Rep. 305 (2000) 1–36.

[17] R. Szalai, D. Roose, Continuation and bifurcation analysis of delay differential equations, in: B. Krauskopf, H. Osinga, J. Galán-Vioque (Eds.), Numerical Continuation Methods for Dynamical Systems, Springer, Dordrecht, 2004, pp. 359–399.

[18] R. Szalai, Knut: A continuation and bifurcation software for delay-differential equations, http://rs1909.github.io/knut/.

[19] D.A. Barton, B. Krauskopf, R.E. Wilson, Collocation schemes for periodic solutions of neutral delay differential equations, J. Difference Equ. Appl. 12 (11) (2006) 1087–1101.

[20] A.A. Andronov, A.A. Vitt, S.E. Khaikin, Theory of Oscillators, in: Adiwes International Series in Physics, Elsevier, 1966.

[21] A.A. Andronov, Theory of Bifurcations of Dynamic Systems on a Plane, Wiley, 1973.

[22] H. Poincaré, Les Méthodes Nouvelles De La Mécanique Céleste, Gauthier-Villars, 1892.

[23] E. Hopf, Abzweigung einer periodischen lösung von einer stationären lösung eines differentialsystems, Berichten Der Mathematisch-Physischen Klasse Der Sächsischen Akademie Der Wissenschaften Zu Leipzig XCIV (1942) 1–22.

[24] J. Guckenheimer, P.J. Holmes, Nonlinear Oscillations, Dynamical Systems, and Bifurcations of Vector Fields, in: Applied Mathematical Sciences, vol. 42, Springer, 1983.

[25] B.D. Hassard, N.D. Kazarinoff, Y.H. Wan, Theory and Applications of Hopf Bifurcation, in: London Mathematical Society Lecture Note Series, Cambridge University Press, 1981.

[26] J.K. Hale, S. M., V. Lunel, Introduction to Functional Differential Equations, in: Applied Mathematical Sciences, Springer-Verlag, New York, 1993.

[27] O. Diekmann, A.S. Gils, S.M.V. Lunel, H.-O. Walther, Delay Equations Functional-, Complex-, and Nonlinear Analysis, Applied Mathematical Sciences, vol. 110, Springer-Verlag New York, 1995.

[28] G. Stépán, Great delay in a predator-prey model, Nonlinear Anal. TMA 10 (9) (1986) 913–929.

[29] T. Kalmár-Nagy, G. Stépán, F. C. Moon, Subcritical Hopf bifurcation in the delay equation model for machine tool vibrations, Nonlinear Dynam. 26 (2001) 121–142.

[30] T.G. Molnar, Z. Dombovari, T. Insperger, G. Stepan, On the analysis of the double Hopf bifurcation in machining processes via centre manifold reduction, Math. Phys. Eng. Sci. 473 (2207) (2017) 913–929.

[31] G. Orosz, G. Stépán, Subcritical Hopf bifurcations in a car-following model with reaction-time delay, Math. Phys. Eng. Sci. 462 (2073) (2006) 2643–2670.

[32] G. Orosz, Hopf bifurcation calculations in delayed systems, Period. Polytech. Mech. Eng. 48 (2) (2004) 189–200.

[33] M. Weedermann, Hopf bifurcation calculations for scalar neutral delay differential equations, Nonlinearity 19 (9) (2006) 2091–2102.

[34] L. Zhang, G. Stépán, Hopf bifurcation analysis of scalar implicit neutral delay differential equation, Electron. J. Qual. Theory Differ. Equ. (62) (2018) 1–9.

[35] X.C. Zeng, Z.L. Xiong, C.J. Wang, Hopf bifurcation for neutral-type neural network model with two delays, Appl. Math. Comput. 282 (2016) 17–31.

[36] D.F. Duan, B. Niu, J.J. Wei, Local and global Hopf bifurcation in a neutral population model with age structure, Math. Methods Appl. Sci. 42 (14) (2019) 4747–4764.

[37] T. Dong, Q. Zhang, Dynamics of a hybrid circuit system with lossless transmission line, IEEE Access 8 (2020) 92969–92976.

[38] L. Zhang, H. Wang, H. Hu, Symbolic computation of normal form for Hopf bifurcation in a neutral delay differential equation and an application to a controlled crane, Nonlinear Dynam. 70 (2012) 463–473.

[39] G. Habib, A. Bártfai, A. Barrios, Z. Dombovari, Bistability and delayed acceleration feedback control analytical study of collocated and non-collocated cases, Nonlinear Dynam. 108 (2022) 2075–2096.

[40] G. Habib, G. Kerschen, G. Stepan, Chatter mitigation using the nonlinear tuned vibration absorber, Int. J. Non-Linear Mech. 91 (2017) 103–112.

[41] A.H. Nayfeh, Order reduction of retarded nonlinear systems–the method of multiple scales versus center-manifold reduction, Nonlinear Dynam. 51 (4) (2008) 483–500.

[42] Y. Song, J.S.M. Vergeest, T.R. Langerak, S. Den Dunnen, M. De Rooij, P. Nyirenda, Freeform shape modifications in selective clay milling, in: ICMA 2004 - Proceedings of the International Conference on Manufacturing Automation: Advanced Design and Manufacturing in Global Competition, Wiley, 2004, pp. 747–754.

[43] Y. Song, J.S.M. Vergeest, T.R. Langerak, Selective clay milling for interactive prototyping, in: Proceedings of the ASME International Design Engineering Technical Conferences and Computers and Information in Engineering Conference, DETC2005, Asme Conference Proceedings, 2005, pp. 1301–1308.

[44] W.C. Tse, Y.H. Chen, A robotic system for rapid prototyping, in: Proceedings of International Conference on Robotics and Automation, IEEE, 1997, pp. 1815–1820.

[45] H.K. Huang, G.C.I. Lin, Rapid and flexible prototyping through a dual-robot workcell, Robot. Comput.-Integr. Manuf. 19 (3) (2003) 263–272.

[46] H. Chen, N. Xi, Automated tool trajectory planning of industrial robots for painting composite surfaces, Int. J. Adv. Manuf. Technol. 35 (7–8) (2008) 680–696.

[47] Y.H. Chen, Y.N. Hu, Implementation of a robot system for sculptured surface cutting. Part 1. Rough machining, Int. J. Adv. Manuf. Technol. 15 (9) (1999) 624–629.

[48] Y.H. Chen, Y.N. Hu, Implementation of a robot system for sculptured surface cutting. Part 2. Finish machining, Int. J. Adv. Manuf. Technol. 15 (9) (1999) 630–639.

[49] S.M. Hazarika, U.S. Dixit, Robotics: History, Trends, and Future Directions, in: Materials Forming, Machining and Tribology, Springer International Publishing, 2018, pp. 213–239.

[50] F. Koenigsberger, J. Tlusty, Machine Tool Structures, in: Springer Tracts in Mechanical Engineering, Springer International Publishing, 2018.
[51] S.A. Tobias, Machine Tool Vibration, Blackie, 1965.
[52] S. Mejri, V. Gagnol, T.-P. Le, L. Sabourin, P. Ray, P. Paultre, Dynamic characterization of machining robot and stability analysis, Int. J. Adv. Manuf. Technol. 82 (2015) 351–359.
[53] A. de Luca, R. Farina, P. Lucibello, On the control of robots with visco-elastic joints, in: Proceedings. 2005 IEEE International Conference on Robotics and Automation, IEEE, 2005, pp. 4297–4302.
[54] L. Sweet, M. Good, Redefinition of the robot motion-control problem, IEEE Control Syst. Mag. 5 (3) (1985) 18–25.
[55] C.C. de Wit, B. Siciliano, G. Bastin, Theory of Robot Control, Springer Science & Business Media, 2012.
[56] J. Munoa, X. Beudaert, K. Erkorkmaz, A. Iglesias, A. Barrios, M. Zatarain, Active suppression of structural chatter vibrations using machine drives and accelerometers, CIRP Ann. 64 (1) (2015) 385–388.
[57] S. Futami, N. Kyura, S. Hara, Vibration absorption control of industrial robots by acceleration feedback, IEEE Trans. Ind. Electron. 30 (3) (1983) 299–305.
[58] L. Cen, S.N. Melkote, Effect of robot dynamics on the machining forces in robotic milling, Proc. Manuf. 10 (2017) 486–496.
[59] G. Xiong, Z. Li, Y. Ding, L. Zhu, Integration of optimized feedrate into an online adaptive force controller for robot milling, Int. J. Adv. Manuf. Technol. 106 (3–4) (2020) 1533–1542.
[60] W.L. Xu, J.D. Han, Joint acceleration feedback control for robots: Analysis, sensing and experiments, Robot. Comput.-Integr. Manuf. 16 (5) (2000) 307–320.
[61] E. Garcia-Benitez, J. Watkins, S. Yurkovich, Nonlinear control with acceleration feedback for a two-link flexible robot, Control Eng. Pract. 1 (6) (1993) 989–997.
[62] B. De Jager, Acceleration assisted tracking control, IEEE Control Syst. Mag. 14 (5) (1994) 20–27.
[63] E. Enikov, G. Stepan, Microchaotic motion of digitally controlled machines, J. Vib. Control 4 (4) (1998) 427–443.
[64] G. Habib, G. Rega, G. Stepan, Delayed digital position control of a single-DoF system and the nonlinear behavior of the act-and-wait controller, J. Vib. Control 22 (2) (2014) 481–495.
[65] H.M. Al-Qahtani, A.A. Mohammed, M. Sunar, Dynamics and control of a robotic arm having four links, Arab. J. Sci. Eng. 42 (2017) 1841–1852.
[66] P.M. Kebria, S. Al-wais, H. Abdi, S. Nahavandi, Kinematic and dynamic modelling of UR5 manipulator, in: 2016 IEEE International Conference on Systems, Man, and Cybernetics, SMC, IEEE, 2016, pp. 4229–4234.
[67] M.H. Korayem, A.M. Shafei, F. Absalan, B. Kadkhodaei, A. Azimi, Kinematic and dynamic modeling of viscoelastic robotic manipulators using timoshenko beam theory: Theory and experiment, Int. J. Adv. Manuf. Technol. 71 (2014) 1005–1018.
[68] G. Habib, G. Rega, G. Stepan, Stability analysis of a two-degree-of-freedom mechanical system subject to proportional–derivative digital position control, J. Vib. Control 21 (8) (2013) 1539–1555.
[69] D. Alazard, J.P. Chretien, Flexible joint control: Robustness analysis of the collocated and non-collocated feedbacks, in: Proceedings. 1993 IEEE/RSJ International Conference on Intelligent Robots and Systems, IEEE, 1993, pp. 2102–2107.
[70] Z. Zuo, X. Ju, Z. Ding, Control of gear transmission servo systems with asymmetric deadzone nonlinearity, IEEE Trans. Control Syst. Technol. 24 (4) (2016) 1472–1479.
[71] M. Jerzy, G. Damian, L. Grzegorz, Control of gear transmission servo systems with asymmetric deadzone nonlinearity, Nonlinear Dynam. 97 (2019) 355–368.
[72] T. Insperger, G. Stepan, Semi-Discretization for Time-Delay Systems, in: Stability and Engineering Applications, Springer-Verlag, New York, 2011.
[73] V.I. Arnold, Geometrical Methods in the Theory of Ordinary Differential Equations, in: Grundlehren der mathematischen Wissenschaften, Springer-Verlag New York, 1988.
[74] J.K. Hale, Theory of Functional Differential Equations, in: Applied Mathematical Sciences, Springer-Verlag, New York, 1977.